A STUDY OF COHERENT NONLINEAR PROCESSES IN DENSE MEDIA WITH CONTINUOUS AND PULSED LASER FIELDS

A Dissertation

by

AIHUA ZHANG

Submitted to the Office of Graduate Studies of
Texas A&M University
in partial fulfillment of the requirements for the degree of

DOCTOR OF PHILOSOPHY

May 2009

Major Subject: Physics

A STUDY OF COHERENT NONLINEAR PROCESSES IN DENSE MEDIA WITH CONTINUOUS AND PULSED LASER FIELDS

A Dissertation

by

AIHUA ZHANG

Submitted to the Office of Graduate Studies of
Texas A&M University
in partial fulfillment of the requirements for the degree of

DOCTOR OF PHILOSOPHY

Approved by:

Chair of Committee,	George R. Welch
Committee Members,	M. Suhail Zubairy
	Alexei Sokolov
	Robert D. Nevels
Head of Department,	Edward Fry

May 2009

Major Subject: Physics

ABSTRACT

A Study of Coherent Nonlinear Processes in Dense Media with Continuous and Pulsed Laser Fields. (May 2009)

Aihua Zhang, B.S., Fudan University;

M.S., Shanghai Jiaotong University

Chair of Advisory Committee: Dr. George. R. Welch

Coherent nonlinear effects such as Electromagnetically Induced Transparency (EIT), Coherent Population Trapping (CPT), and Slow light are studied in thermal Rb vapor by both continuous and pulsed laser fields. This work primarily includes three parts: (I) mode-locked rubidium laser and its applications (II) enhanced coupling between optical and sound waves in the forward direction via ultra-slow light (III) optical steering via ultra-slow light in rubidium vapor.

In part(I), I describe the construction and study of a mode-locked rubidium laser operating at the Rb D1 line using an active mode-locking technique inside the laser cavity. The mode-locked laser field is used to observe coherent effects in a dense rubidium gas.

In part(II), I experimentally demonstrate enhanced acoustic-optic coupling that occurs when the velocity of sound is close to the group velocity of light. Dragging of the light by effective motion of the gas in a Rb cell is the origin of enhanced coupling. Good agreement between theory and experiment is found.

In part(III), I experimentally demonstrate optical beam deflection in coherently driven rubidium vapor due to the steep refraction index profile in the region of EIT.

To my parents Xinqi Zhang and Huizhen Chen

ACKNOWLEDGMENTS

There are many people who contributed to this work presented here. I am grateful to everyone who helped and supported me.

First, I would like to express my deepest sense of respect and sincere gratitude to my advisor, Prof. George R. Welch, who guided me into the physics world of my research with his profound knowledge and constant support during my stay at Texas A&M University. His deep insight to the key of the problem has been a source of inspiration of me. I want to thank Dr. Vladimir A Sautenkov who taught me everything I should know about experimental work and helped me to get started in the research field. I would like to wholeheartedly thank Dr. Yuri Rostovtsev for his constant encouragement and inspiration and his enthusiasm and talent during this Ph.D. work. I also would like to acknowledge the important contributions of Dr. Irina Novikova and Dr. Eugeniy E. Mikhailov who shared their ideas and lead me into this research field. I am very grateful for the honor of meeting and would like to acknowledge the important contributions of Dr. Marlan O. Scully, Dr. M. Suhail Zubairy, Dr. Alexei Sokolov, Dr. Robert D. Nevels and Dr. Philip Hemmer.

Also, I would like to gratefully acknowledge helpful discussions in physics with Dr. Paul S. Hsu, Xi Wang, Hebin Li, Dr. Hui Chen, Dr. Miaochan Zhi, Ling Wang.

I'd like to thank my parents who taught me the true value of hard work with their endless love and support. I am very thankful to my husband for his patience and constant moral and physical support. I give thanks for my son, Anthony, who gives me new meaning of life. This thesis is dedicated to them.

TABLE OF CONTENTS

CHAPTER Page

LIST OF FIGURES

FIGURE Page

FIGURE Page

FIGURE Page

FIGURE Page

CHAPTER I

INTRODUCTION

Coherent nonlinear effects such as Electromagnetically Induced Transparency (EIT) and Coherent Population Trapping (CPT) [1] attract attention due to the development of new applications such as atomic clocks [2], high precision spectroscopy [3], large Kerr nonlinearities [4] and others. After about thirty years of exciting developments in this research area, many coherent nonlinear effects have been successfully demonstrated in different media by different laser sources. The first observation was by Adriano Gozzini and his coworkers in 1976 [5], where CPT was discovered when the two-photo detuning of two laser fields was matched to the atomic level splitting, causing the fluorescence to be highly suppressed. While EIT is the same mechanism which includes a weak probe field and a strong drive field. Both CPT and EIT can be explained with a picture of bright and dark states, or coherent superpositions of atomic energy levels. If atoms are pumped into the dark state which does not interact with electromagnetic field, fluorescence is highly suppressed and transmission of the probe field is significantly increased.

Many new phenomena has been discovered in the EIT regime that depend on the modified properties of medium. After about thirty years of exciting developments, hundreds of experiments and theoretical predictions are devoted to EIT and its applications. Different configurations are theoretically suggested and experimentally demonstrated, such as the Λ scheme, which has 2 ground states and 1 upper state with two fields coupling, and the V scheme, which has 2 upper states and 1 ground state coupled by two fields, and the ladder scheme, which has two laser fields coupling to the three energy states.

An important EIT coherence effect is the presence of resonance features with sub-

---

This dissertation follows the style of Physical Review A.

natural resonance width. This has been successfully demonstrated in different media by continuous-wave or pulsed lasers, such as with atomic or molecular gases (at room temperature [6] [7], with cold atoms [8], with cold atoms and molecules [9]), with rare-earth ion doped solids [10] [11] and semiconductor quantum wells [12]. Such narrow resonances indict a bright future for many applications, such as magnetometry [13], precision spectroscopy [14] and frequency standards [15]. Detailed information can be found in the recent review paper [16].

Steep dispersion also accompanies the narrow EIT resonance, which enables the observation of low group velocity as low as several meters per second [4] [17] [18] [19]. Using EIT to slow the group velocity well below the speed of sound has been demonstrated experimentally in both cold [20] and hot [18] atomic gases as well as in crystals doped by rare-earth ions [21]. Other techniques have also produced very low optical group velocity, including nonlinear magneto-optical polarization rotation [22], hole burning in ruby crystals [23], and photo refractive effects in crystals [24]. Also, slow and halted light pulses have been suggested in quantum computing research [25] [26] [27] [28].

This dissertation addresses coherent nonlinear processes in dense media by continuous and pulsed laser fields in three main parts: (1) coherent effects using a mode-locked rubidium laser (2) enhanced coupling between optical and sound waves in the forward direction via ultra-slow light (3) optical steering via ultra-slow light in rubidium vapor.

The modern concept of the interaction between light and matter can be explained by a combined theory using Maxwell's equations and quantum mechanics. In this section, I present the general methods to describe the interaction between light and atoms relevant to this dissertation.

A. Maxwell's equations

Maxwell's equations that describe the propagation of the electromagnetic field in a medium can be written as [29]:

$$\nabla \cdot D = 0 \tag{1.1}$$

$$\nabla \cdot B = 0 \tag{1.2}$$

$$\nabla \times E = -\frac{1}{c}\frac{\partial B}{\partial t} \tag{1.3}$$

$$\nabla \times H = \frac{1}{c}\frac{\partial D}{\partial t} \tag{1.4}$$

If no external charge or current is present, we can set $\rho = J = 0$. We also set:

$$D = E + 4\pi P \tag{1.5}$$

$$B = H + 4\pi M \tag{1.6}$$

where P and M are the electric dipole moment per unit volume, and magnetic moment per unit volume, respectively. If we confine our interest only in nonmagnetic media with $M = 0$, we have:

$$\nabla \cdot E + 4\pi \nabla \cdot P = 0 \tag{1.7}$$

and with $B = H$, Maxwell equations can be easily combined into,

$$\nabla^2 E - \nabla(\nabla \cdot E) - \frac{1}{c^2}\frac{\partial^2 E}{\partial t^2} - \frac{4\pi \partial^2 P}{c^2 \partial t^2} = 0 \tag{1.8}$$

This is the relationship between the dipole moment per unit volume P and the macroscopic electric field E.

In an atomic vapor medium characterized by the absence of free charges $\rho = 0$

and $\vec{j} = 0$, the equation of the electric component of the light field can be written as:

$$\nabla^2 E - \frac{1}{c^2}\frac{\partial^2 E}{\partial t^2} = \frac{4\pi\partial^2 P}{c^2\partial t^2} \tag{1.9}$$

Let us consider a plane wave which is circularly polarized along the x-y plane, and propagating along the z direction

$$E(\vec{z}, t) = \varepsilon(z, t)e^{ikz-ivt}\vec{\epsilon} + C.C. \tag{1.10}$$

where, $\varepsilon(z, t)$ is the amplitude of the field, $k = 2\pi/\lambda$ is the propagation wave vector of the field with wavelength λ and oscillation frequency v. Also, the response of medium can be written as

$$\vec{P}(z, t) = P(z, t)e^{ikz-ivt}\vec{\epsilon} + C.C. \tag{1.11}$$

The induced polarization can be expanded into a Taylor series in the power of the laser field $\vec{E}$. In conventional linear optics, the induced polarization linearly depends on the external electric field

$$P(\vec{z}, t) = \vec{\epsilon}\chi(v)\varepsilon(z)e^{ikz-ivt} + C.C. \tag{1.12}$$

We assume that changes in the amplitude of the electromagnetic wave take place on a time scale much larger than one cycle of the oscillations, also distance change is much longer than the wavelength. This is called as the *slowly varying amplitude approximation.*

$$\frac{\partial\varepsilon}{\partial z} \ll k\varepsilon; \qquad \frac{\partial\varepsilon}{\partial t} \ll v\varepsilon; \qquad \frac{\partial P}{\partial t} \ll vP; \qquad \frac{\partial P}{\partial z} \ll kP \tag{1.13}$$

Thus equation (1.9) can be written as:

$$\frac{\partial\varepsilon}{\partial z} + \frac{1}{c}\frac{\partial\varepsilon}{\partial t} = 2i\pi kP \tag{1.14}$$

B. Nonlinear response of matter

As we know, the laboratory fields of interest are very small compared to the electric fields which experienced by electrons in the atoms and molecules. Therefore, we can expand the dipole moment per unit volume in a Taylor series in powers of the macroscopic field E:

$$P_\alpha(r,t) = P_\alpha^{(0)} + \sum_\beta (\frac{\partial P_\alpha}{\partial E_\beta})_0 E_\beta + \frac{1}{2!}\sum_{\beta\gamma}(\frac{\partial^2 P_\alpha}{\partial E_\beta \partial E_\gamma \partial E_\beta})_0 E_\beta E_\gamma + \frac{1}{3!}\sum_{\beta\gamma\delta}(\frac{\partial^3 P_\alpha}{\partial E_\gamma \partial E_\beta \partial E_\delta})_0 E_\beta E_\gamma E_\delta + \cdots \tag{1.15}$$

For most materials, the electric dipole moment per unit volume in zero electric field vanishes. Therefore, the dipole moment is induced by an external field.

We are interested in time-dependent phenomena in response to externally applied fields.

$$P_\alpha(r,t) = \sum_\beta \chi^{(1)}_{\alpha\beta} E_\beta(r,t) + \sum_{\beta\gamma} \chi^{(2)}_{\alpha\beta\gamma} E_\beta(r,t) E_\gamma(r,t) + \sum_{\beta\gamma\delta} \chi^{(3)}_{\alpha\beta\gamma\delta} E_\beta(r,t) E_\gamma(r,t) E_\delta(r,t) + \cdots \tag{1.16}$$

Where $\chi^{(1)}_{\alpha\beta}$ is the linear susceptibility, $\chi^{(2)}_{\alpha\beta\gamma}$ is called the second-order susceptibility, $\chi^{(3)}_{\alpha\beta\gamma\delta}$ is the third-order susceptibility, and so on. Those second, third and higher order susceptibilities are responsible for the nonlinear response of the electric field.

C. Atom-field interaction Hamiltonian

The quantum mechanical state should satisfy the Schrödinger equation [30]:

$$i\hbar \frac{\partial |\psi\rangle}{\partial t} = H|\psi\rangle \tag{1.17}$$

where $|\psi\rangle$ represents the quantum mechanical state in the atomic system and H is the Hamiltonian operator of the system. There is another alternative way to deal with

atomic systems, which is to use the density operator $\hat{\rho}$.

$$\hat{\rho} = |\psi\rangle\langle\psi| = \sum_{i,j} \rho_{i,j}|i\rangle\langle j| \tag{1.18}$$

where $\rho_{i,j}$ is the matric elements in the $\{|i\rangle\}$ basis. Using the density matrix the Schröinger equation can be written as [31]:

$$\frac{d\rho}{dt} = -\frac{i}{\hbar}[H, \rho] \tag{1.19}$$

We separate the Hamiltonian into two parts, H_0 is the Hamiltonian in the absence of any external field, and H_I is the interaction part of the atom with the external electro-magnetic field.

$$H = H_0 + H_I \tag{1.20}$$

In the case of atom-field interaction, $H_I = -e\vec{r} \cdot \vec{E}$,

$$H_{oij} = \hbar\omega_i \delta_{ij}|i\rangle\langle j| \tag{1.21}$$

$$H_{Iij} = \sum_k d_{ijk} E_{t_k}(t)|i\rangle\langle j| \tag{1.22}$$

where d_{ijk} is dipole moment of transition $i \rightarrow j$ for polarization.

If the decay of the atomic state is included in our system, the decay operator Γ can be added to the Hamiltonian as:

$$\frac{d\rho}{dt} = -\frac{i}{\hbar}[H, \rho] - \frac{1}{2}\{\Gamma, \rho\} \tag{1.23}$$

where the matrix elements of Γ are

$$\Gamma_{ij} = \frac{1}{2}(\gamma_i + \gamma_j) + \gamma_{ij} \tag{1.24}$$

whereγ_i and γ_j are the population decay rate of the state $|i\rangle$ and $|j\rangle$, and γ_{ij} is dephasing rate due to phase relaxation.

D. Maxwell - Schrödinger equations

The study of light propagation inside the medium has been a major subject in physics. An important mathematic work to address the evolution of the state of light propagating through the medium is the Maxwell - Schrödinger equations, a self-consistent set of equations for the matter and the field [31]. By applying the technique, the density matrix is used to take care of the statistics involved in obtaining the macroscopic polarization of the whole medium by an individual dipole moment.

In the previous section, we had:

$$\dot{\rho} = -\frac{i}{\hbar}[H, \rho] \tag{1.25}$$

and if we include decay processes, then the density matrix equation of motion can be written as:

$$\dot{\rho} = -\frac{i}{\hbar}[H, \rho] - \frac{1}{2}\{\Gamma, \rho\} \tag{1.26}$$

where Γ is the relaxation matrix with:

$$\langle n|\Gamma|m\rangle = \gamma_n \delta_{nm} \tag{1.27}$$

Therefore, the equation of motion for the density matrix in the ij matrix element can be written as:

$$\dot{\rho_{ij}} = -\frac{i}{\hbar}\sum_k (H_{ik}\rho_{kj} - \rho_{ik}H_{kj}) - \frac{1}{2}\sum_k (\Gamma_{ik}\rho_{kj} + \rho_{ik}\Gamma_{kj}) \tag{1.28}$$

For individual atoms, we can consider the interaction of an electromagnetic field using the density operator,

$$\rho(z, t, t_0) = \sum_{\alpha\beta} \rho_{\alpha\beta}(z, t, t_0)|\alpha\rangle\langle\beta| \tag{1.29}$$

with the density matrix elements $\rho_{\alpha\beta}(z, t, t_0)$ at time t and position z initially interacting with the field at time t_0. If the atoms are pumped into the field at the rate

of $r_a(z,t_0)$, the macroscopic polarization of the medium $P(z,t)$ can be written as the following:

$$P(z,t) = \int_{-\infty}^{t} dt_0 r_a(z,t_0) Tr[\hat{\wp}\rho(z,t,t_0)] = \sum_{\alpha\beta} \int_{-\infty}^{t} dt_0 r_a(z,t_0\rho_{\alpha\beta})(z,t,t_0)\wp_{\alpha\beta} \quad (1.30)$$

with $\wp$ the dipole moment operator. Therefore, off-diagonal elements of the population matrix elements determine the macroscopic polarization.

The Maxwell-Schrödinger equations for slowly varying fields which are given in the above section, and the equations of motion for the elements of the population matrix, is self-consistent, and addresses the interaction of the radiation field with an ensemble of atoms.

CHAPTER II

PROPERTY OF EIT AND SLOW LIGHT IN THREE LEVEL SYSTEMS

A. Electromagnetically induced transparency

Electromagnetically induced transparency(EIT) is an optical nonlinearity which changes the medium transparency by coherent lights sources. In the case of the three level Λ system, EIT causes a modification of the absorption profile of an atomic transition if the upper energy level is coupled coherently to a third level by a strong laser field [32]. In some circumstances, absorption of the probe field can be substantially reduced. This nonlinear effect is caused by the interference between the coherence excited in the atomic levels by the electromagnetic fields and leads to an initially highly opaque medium being almost transparent.

In this chapter, the physical basis of EIT and the related phenomena of slow light is studied. A physical picture of these effects will be provided.

Three-level atomic systems are involved when we study EIT and other related atomic coherence phenomena. These three levels normally require two pairs of levels that are dipole transition allowed, and leave the third with no dipole allowed transition. The three typical level configurations as shown in Fig. 1: (1) Ladder scheme or cascade scheme (2) Λ scheme (3) V scheme.

1. Λ configuration

Firstly, let us consider the three level Λ configuration, which is made up of two lower energy levels and one upper energy level interacting with two electro-magnetic fields, called the probe field and pump field. The picture is shown in the Fig. 2.

The Hamiltonian for this system is given by:

$$H = \hbar\omega_a|a\rangle\langle a| + \hbar\omega_b|b\rangle\langle b| + \hbar\omega_c|c\rangle\langle c| - \hbar(\Omega_d e^{-iv_d t}|a\rangle\langle c| + \Omega_p e^{-iv_p t}|a\rangle\langle b|) + C.C. \quad (2.1)$$

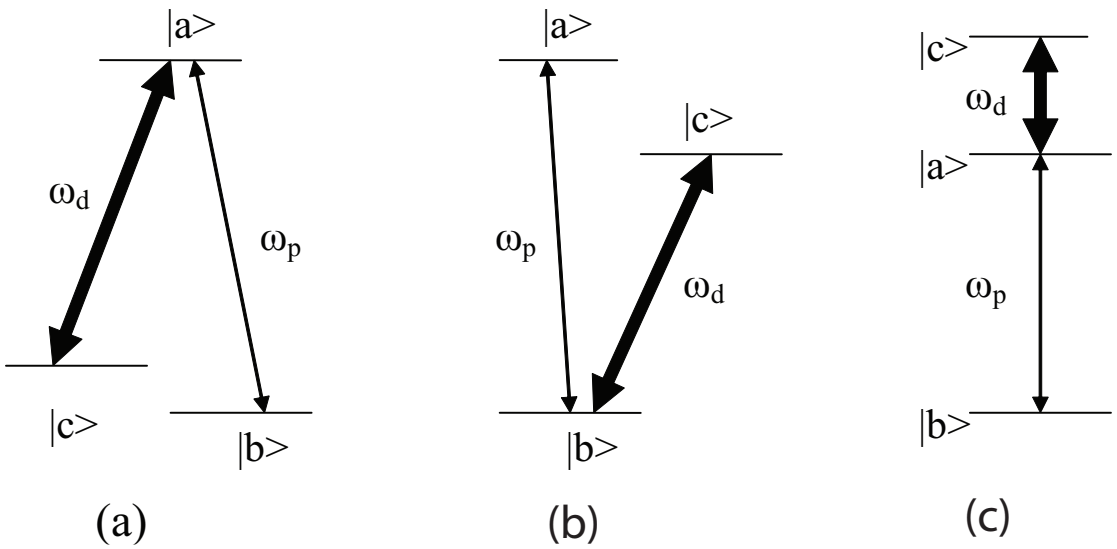

Fig. 1. Three level EIT configurations: (a) Λ-scheme, Ω_d is the strong drive field and Ω_p is the weak probe field. (b) V-scheme (c) Ladder scheme or cascade scheme.

Ω is the Rabi frequency of driving or probe field,

$$\Omega_d = \frac{d_{ac}\varepsilon_d}{\hbar}; \qquad \Omega_p = \frac{d_{ab}\varepsilon_p}{\hbar} \tag{2.2}$$

By using the rotating wave approximation, the evolution of the density matrix is given as:

$$\dot{\rho_{aa}} = -i\Omega_p^*\rho_{ab} + i\Omega_p\rho_{ba} - i\Omega_d^*\rho_{ac} + i\Omega_d\rho_{ca} - 2\gamma\rho_{aa} \tag{2.3}$$

$$\dot{\rho_{bb}} = i\Omega_p^*\rho_{ab} - i\Omega_p\rho_{ba} + \gamma\rho_{aa} - \gamma_{bc}\rho_{bb} + \gamma_{bc}\rho_{cc} \tag{2.4}$$

$$\dot{\rho_{cc}} = i\Omega_d^*\rho_{ac} - i\Omega_d\rho_{ca} + \gamma\rho_{aa} - \gamma_{bc}\rho_{cc} + \gamma_{bc}\rho_{bb} \tag{2.5}$$

$$\dot{\rho_{ab}} = -\Gamma_{ab}\rho_{ab} + i\Omega_p(\rho_{bb} - \rho_{aa}) + i\Omega_d\rho_{cb} \tag{2.6}$$

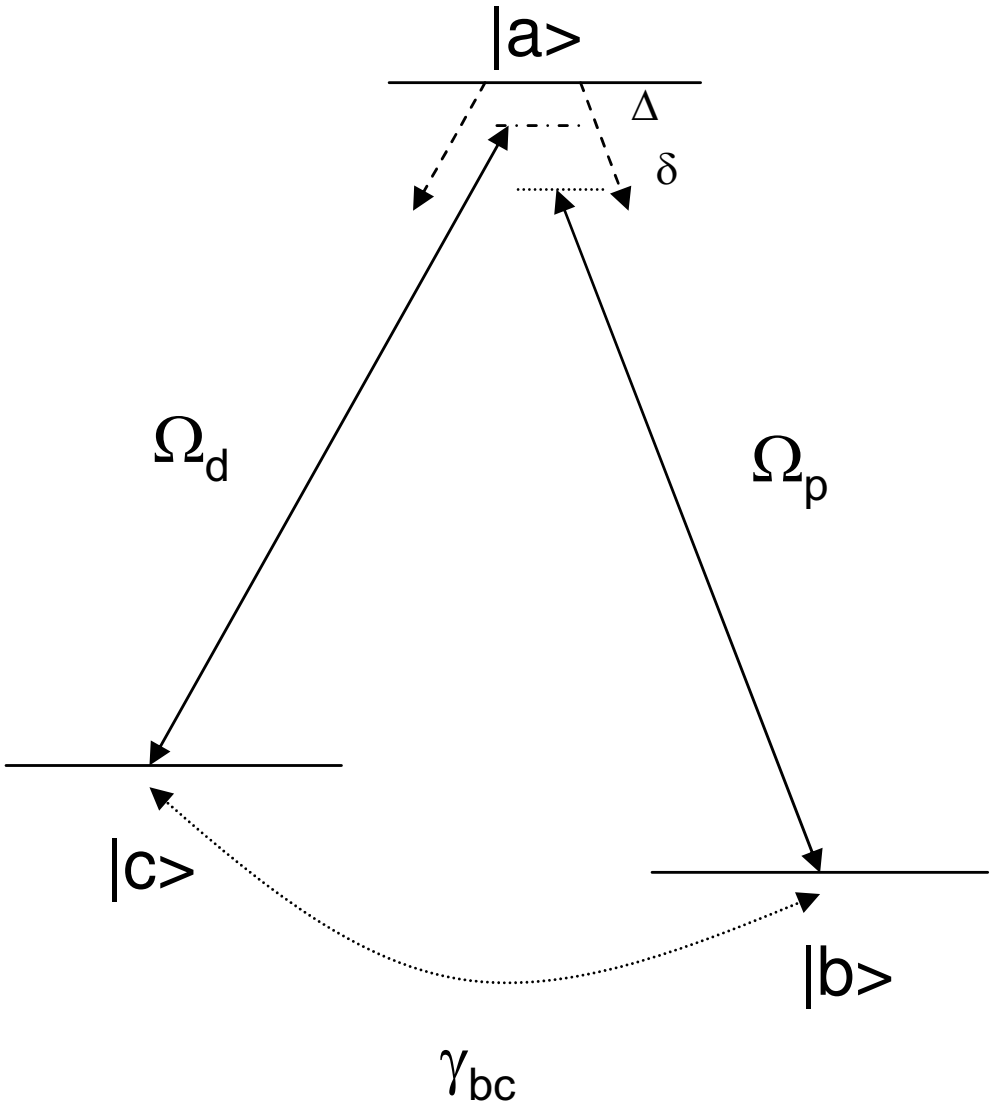

Fig. 2. Three level Λ configuration.

$$\dot{\rho_{ca}} = -\Gamma_{ca}\rho_{ca} + i\Omega_d^*(\rho_{aa} - \rho_{cc}) - i\Omega_p^*\rho_{cb} \tag{2.7}$$

$$\dot{\rho_{cb}} = -\Gamma_{cb}\rho_{cb} - i\Omega_p\rho_{ca} + i\Omega_d^*\rho_{ab} \tag{2.8}$$

with

$$\Gamma_{ab} = \gamma + i(\Delta + \delta) \tag{2.9}$$

$$\Gamma_{ca} = \gamma - i\Delta \tag{2.10}$$

$$\Gamma_{cb} = \gamma_{bc} + i\delta \tag{2.11}$$

The analytic solution for $\rho_{aa}, \rho_{bb}, \rho_{cc}, \rho_{ab}, \rho_{ca}, \rho_{cb}$ can be given if we are working in the steady state regime.

$$\rho_{ab} = i\Omega_p \frac{(\rho_{bb} - \rho_{aa})(\Gamma_{ac}^*\Gamma_{cb} + |\Omega_p|^2) + |\Omega_d|^2(\rho_{aa} - \rho_{cc})}{\Gamma_{ab}\Gamma_{ac}^*\Gamma_{cb} + \Gamma_{ac}^*|\Omega_d|^2 + \Gamma_{ab}|\Omega_p|^2} \tag{2.12}$$

$$\rho_{ca} = i\Omega_d^* \frac{(\rho_{aa} - \rho_{cc})(\Gamma_{ab}^*\Gamma_{cb} + |\Omega_d|^2) + |\Omega_p|^2(\rho_{bb} - \rho_{aa})}{\Gamma_{ab}\Gamma_{ac}^*\Gamma_{cb} + \Gamma_{ac}^*|\Omega_d|^2 + \Gamma_{ab}|\Omega_p|^2} \tag{2.13}$$

$$\rho_{cb} = i\Omega_p\Omega_d^* \frac{(\rho_{aa} - \rho_{cc})\Gamma_{ab} - (\rho_{bb} - \rho_{aa})\Gamma_{ac}^*}{\Gamma_{ab}\Gamma_{ac}^*\Gamma_{cb} + \Gamma_{ac}^*|\Omega_d|^2 + \Gamma_{ab}|\Omega_p|^2} \tag{2.14}$$

2. V configuration

Next, we consider the V configuration, made up of two upper energy levels and one lower energy level interacting with two electro-magnetic fields: probe field and pump field. The picture is shown in Fig. 3. The Hamiltonian is the following:

$$H_o = \hbar\omega_a|a\rangle\langle a| + \hbar\omega_b|b\rangle\langle b| + \hbar\omega_c|c\rangle\langle c| \tag{2.15}$$

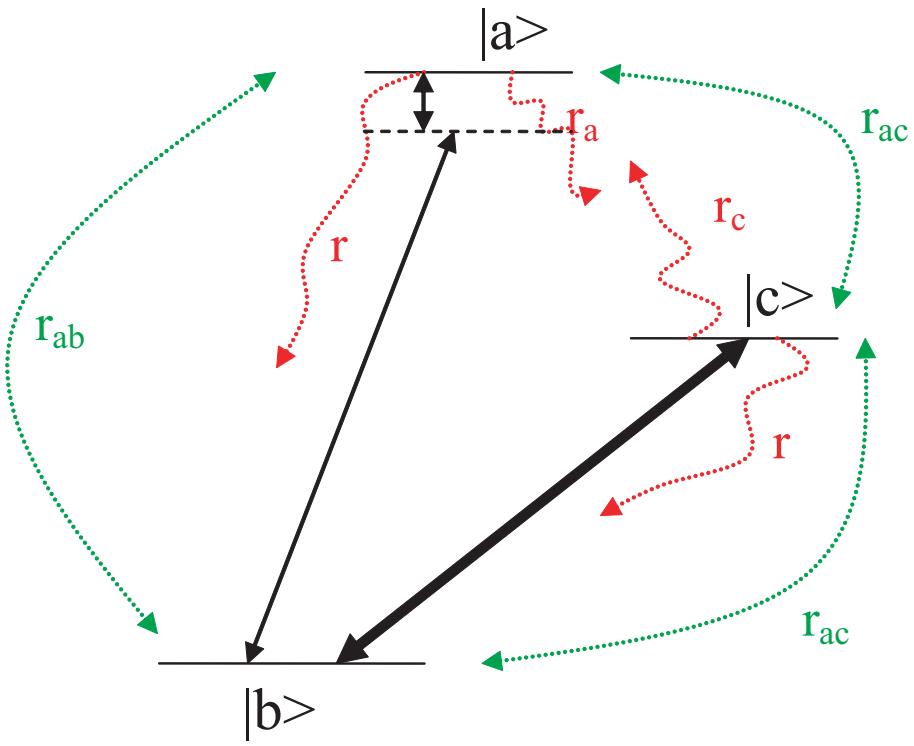

Fig. 3. Three level V configuration with strong field coupling the state $|c\rangle$ and the state $|b\rangle$, and probe weak field coupling upper state $|a\rangle$ and the state $|b\rangle$. r is the decay rate of upper energy level to the group state, r_a, r_c are the decay rate between the states $|a\rangle$ and $|c\rangle$. r_{ac}, r_{ab}, r_{bc} are the dephasing decay rates between energy levels.

$$H_I = -\hbar(\Omega_{R1}e^{-iv_1t}|a\rangle\langle b| + \Omega_{R2}e^{-iv_2t}|c\rangle\langle b|) + H.C. \tag{2.16}$$

Using the Liouville equation,

$$\dot{\rho_{aa}} = -(\gamma + \gamma_a)\rho_{aa} + \gamma_c\rho_{cc} - i\Omega^*_{R1}e^{iv_1t}\rho_{ab} + i\Omega_{R1}e^{-iv_1t}\rho_{ba} \tag{2.17}$$

$$\dot{\rho_{bb}} = \gamma(\rho_{aa} + \rho_{cc}) - i\Omega_{R1}e^{-iv_1t}\rho_{ba} - i\Omega^*_{R2}e^{-iv_2t}\rho_{bc} + i\Omega^*_{R1}e^{iv_1t}\rho_{ab} + i\Omega_{R2}e^{iv_2t}\rho_{cb} \tag{2.18}$$

$$\dot{\rho_{cc}} = -(\gamma + \gamma_c)\rho_{aa} + \gamma_c\rho_{aa} - i\Omega^*_{R2}e^{iv_2t}\rho_{cb} + i\Omega_{R2}e^{-iv_2t}\rho_{bc} \tag{2.19}$$

$$\dot{\rho_{ab}} = -(\frac{\gamma + \gamma_a}{2} + \gamma^{(ab)}_{ph} + i\omega_{ab})\rho_{ab} - i\Omega_{R1}e^{-iv_1t}(\rho_{aa} - \rho_{bb}) - i\Omega^*_{R2}e^{-iv_2t}\rho_{ac} \tag{2.20}$$

$$\dot{\rho_{bc}} = -(\frac{\gamma + \gamma_c}{2} + \gamma^{(cb)}_{ph} - i\omega_{cb})\rho_{bc} + i\Omega^*_{R1}e^{-iv_1t}\rho_{ac} + i\Omega_{R2}e^{iv_2t}(\rho_{cc} - \rho_{bb}) \tag{2.21}$$

$$\dot{\rho_{ac}} = -(\frac{2\gamma + \gamma_c + \gamma_a}{2} + \gamma^{(ca)}_{ph} + i\omega_a c)\rho_{ac} - i\Omega_{R2}e^{iv_2t}\rho_{ab} + i\Omega_{R1}e^{-iv_1t}\rho_{bc} \tag{2.22}$$

With slow rotation amplitude proximation,

$$\rho_{ab} = \tilde{\rho_{ab}}e^{-iv_1t} \tag{2.23}$$

$$\rho_{bc} = \tilde{\rho_{bc}}e^{iv_2t} \tag{2.24}$$

$$\rho_{ac} = \tilde{\rho_{ac}}e^{-i(v_1 - v_2)t} \tag{2.25}$$

Therefore, the above equations can be written as:

$$\dot{\tilde{\rho_{aa}}} = -(\gamma + \gamma_a)\tilde{\rho_{aa}} + \gamma_c\tilde{\rho_{cc}} - i\Omega_{R1}^*\tilde{\rho_{ab}} + i\Omega_{R1}\tilde{\rho_{ba}} \tag{2.26}$$

$$\dot{\tilde{\rho_{bb}}} = \gamma(\tilde{\rho_{aa}} + \tilde{\rho_{cc}}) - i\Omega_{R1}\tilde{\rho_{ba}} - i\Omega_{R2}^*\tilde{\rho_{bc}} + i\Omega_{R1}^*\tilde{\rho_{ab}} + i\Omega_{R2}\tilde{\rho_{cb}} \tag{2.27}$$

$$\dot{\tilde{\rho_{cc}}} = -(\gamma + \gamma_c)\tilde{\rho_{aa}} + \gamma_c\tilde{\rho_{aa}} - i\Omega_{R2}^*\tilde{\rho_{cb}} + i\Omega_{R2}\tilde{\rho_{bc}} \tag{2.28}$$

$$\dot{\tilde{\rho_{ab}}} = -(\frac{\gamma + \gamma_a}{2} + \gamma_{ph}^{(ab)} + i\omega_a b - iv_1)\tilde{\rho_{ab}} - i\Omega_{R1}(\tilde{\rho_{aa}} - \tilde{\rho_{bb}}) - i\Omega_{R2}^*\tilde{\rho_{ac}} \tag{2.29}$$

$$\dot{\tilde{\rho_{bc}}} = -(\frac{\gamma + \gamma_c}{2} + \gamma_{ph}^{(cb)} - i\omega_c b_i v_2)\tilde{\rho_{bc}} + i\Omega_{R1}^*\tilde{\rho_{ac}} + i\Omega_{R2}(\tilde{\rho_{cc}} - \tilde{\rho_{bb}}) \tag{2.30}$$

$$\dot{\tilde{\rho_{ac}}} = -(\frac{2\gamma + \gamma_c + \gamma_a}{2} + \gamma_{ph}^{(ca)} + i\omega_a c - i(v_1 - v_2))\tilde{\rho_{ac}} - i\Omega_{R2}\tilde{\rho_{ab}} + i\Omega_{R1}\tilde{\rho_{bc}} \tag{2.31}$$

with the parameters:

$$\Gamma_{ab} = \frac{\gamma + \gamma_a}{2} + \gamma_{ph}^{(ab)} + i\omega_{ab} - iv_1 \tag{2.32}$$

$$\Gamma_{bc} = \frac{\gamma + \gamma_c}{2} + \gamma_{ph}^{(cb)} - i\omega_{cb} + iv_2 \tag{2.33}$$

$$\Gamma_{ac} = \frac{2\gamma + \gamma_a + \gamma_c}{2} + \gamma_{ph}^{(ca)} + i\omega_{ac} - i(v_1 - v_2) \tag{2.34}$$

And the equations for steady state are:

$$-(\gamma + \gamma_a)\rho_{aa} + \gamma_c\rho_{cc} - i\Omega_{R1}^*\rho_{ab} + i\Omega_{R1}\rho_{ba} = 0 \tag{2.35}$$

$$\gamma(\rho_{aa}+\rho_{cc})-i\Omega_{R1}\rho_{ba}-i\Omega_{R2}^{*}\rho_{bc}+i\Omega_{R1}^{*}\rho_{ab}+i\Omega_{R2}\rho_{cb}=0 \tag{2.36}$$

$$-(\gamma+\gamma_c)\rho_{aa}+\gamma_c\rho_{aa}-i\Omega_{R2}^{*}\rho_{cb}+i\Omega_{R2}\rho_{bc}=0 \tag{2.37}$$

$$-\Gamma_{ab}\rho_{ab}-i\Omega_{R1}(\rho_{aa}-\rho_{bb})-i\Omega_{R2}^{*}\rho_{ac}=0 \tag{2.38}$$

$$-\Gamma_{bc}\rho_{bc}+i\Omega_{R1}^{*}\rho_{ac}+2\Omega_{R2}(\rho_{cc}-\rho_{bb})=0 \tag{2.39}$$

$$-\Gamma_{ac}\rho_{ac}-i\Omega_{R2}\rho_{ab}+i\Omega_{R1}\rho_{bc}=0 \tag{2.40}$$

If drive field is much stronger than probe field, $|\Omega_{R1}|^2 \ll |\Omega_{R2}|^2$, we could solve these equations with simple solutions,

$$\rho_{ab}=i\Omega_{R1}\frac{(\rho_{aa}-\rho_{bb})-\frac{|\Omega_{R2}|^2}{\Gamma_{ab}\Gamma_{bc}}(\rho_{bb}-\rho_{cc})}{\Gamma_{ab}+\frac{|\Omega_{R2}|^2}{\Gamma_{ac}}} \tag{2.41}$$

$$\rho_{bc}=i\Omega_{R2}\frac{(\rho_{cc}-\rho_{bb})}{\Gamma_{bc}} \tag{2.42}$$

And further with $\rho_{aa}+\rho_{bb}+\rho_{cc}=1$, we can solve $\rho_{aa},\rho_{bb},\rho_{cc}$:

$$\rho_{aa}=\frac{2|\Omega_{R2}|^2}{2|\Omega_{R2}|^2+\gamma\Gamma_{bc}+\gamma\Gamma_{bc}\frac{\gamma+\gamma_a}{\gamma_c}+4|\Omega_{R2}|^2\frac{\gamma+\gamma_a}{\gamma_c}} \tag{2.43}$$

$$\rho_{bb}=\frac{2|\Omega_{R2}|^2\frac{\gamma+\gamma_a}{\gamma_c}+\gamma\Gamma_{bc}+\gamma\Gamma_{bc}\frac{\gamma+\gamma_a}{\gamma_c}}{2|\Omega_{R2}|^2+\gamma\Gamma_{bc}+\gamma\Gamma_{bc}\frac{\gamma+\gamma_a}{\gamma_c}+4|\Omega_{R2}|^2\frac{\gamma+\gamma_a}{\gamma_c}} \tag{2.44}$$

$$\rho_{cc}=\frac{2|\Omega_{R2}|^2\frac{\gamma+\gamma_a}{\gamma_c}}{2|\Omega_{R2}|^2+\gamma\Gamma_{bc}+\gamma\Gamma_{bc}\frac{\gamma+\gamma_a}{\gamma_c}+4|\Omega_{R2}|^2\frac{\gamma+\gamma_a}{\gamma_c}} \tag{2.45}$$

3. Dark state and EIT line shape

The previous sections give equations describing the time-dependent density matrix elements with monochromatic coupling fields and ignoring collisional and Doppler broadening. To understand the modification of optical properties, we first need to examine the linear and nonlinear optical susceptibilities. The macroscopic polarization can be related to the microscopic coherence (density matrix elements) via the expression $P_{ab} = N\wp_{ab}\rho_{ab}$, where N is the number of equivalent atoms in the ground state within the medium, and $\wp_{ab}$ is the dipole matrix element. This relation is correct for a medium sufficiently dilute so that dipole-dipole coupling between different atoms can be ignored. Therefore, the imaginary and real parts of the linear susceptibility can be directly related to ρ_{ab}, by $P_{ab}(\omega) = \varepsilon_0\chi(\omega)E$, which is referred to semiclassical approach. In the case where the drive field is strong compared to probe field, level $|c\rangle$ is the depleted by applied driving field, and level $|b\rangle$ is fully populated via the decay from upper state $|a\rangle$. Also referring to Equ. [2.12], we can ignore the term $|\Omega_p|^2$ compared with $|\Omega_d|^2$,

$$\rho_{ab} = i\Omega_p \frac{\Gamma_{cb}}{\Gamma_{ab}\Gamma_{cb} + |\Omega_d|^2} \tag{2.46}$$

The probe field susceptibility of the media can be written as:

$$\begin{aligned} \chi &= -\kappa\rho_{ab}/\Omega_p \\ &= i\frac{\kappa\Gamma_{cb}}{\Gamma_{ab}\Gamma_{cb} + |\Omega_d|^2} \\ &= \frac{i\kappa}{\gamma}\left(1 - \frac{\frac{|\Omega_d|^2}{\gamma}}{\gamma_{bc} + \frac{|\Omega_d|^2}{\gamma} + i\delta}\right) \end{aligned}$$

where $\kappa = 3N\lambda^2\gamma_r/8\pi^2$ and assuming $\Delta, \delta, \gamma_{cb} \ll \gamma$.

The absorption of the probe field vanishes at exact resonance if the drive field is applied as shown in the Fig. 4 [33]. The real part of the susceptibility determines the refractive index, and the imaginary part of susceptibility determines the dissipation

of the field by the atom.

Fig. 4 shows the imaginary and real parts of the linear susceptibility as a function of the probe field detuning for both two-level system and the three-level EIT system. The real part of the susceptibility is proportional to the difference between the refractive index in the medium and that in free space. The slope is very steep, giving rise to very slow group velocities and the possibility of other new applications. The imaginary part is proportional to the loss in the medium with zero at line center and varies quadratically as a function of detuning of probe field for small region.

The reduction in absorption is not caused by some effective detuning; instead it is caused by the interference. The interference can be constructive or destructive, and the physics underlying the cancelation of absorption in EIT is due to destructive interference. We could use a coherent superposition of atomic states, usually called the dark state, to briefly explain EIT. In other words, if an atom is prepared in a coherent superposition of states, under some conditions absorption can be canceled. Therefore, the medium is transparent to the incident field even at the resonance of the transition.

Still considering a Λ scheme, the atomic wave function can be written as the following:

$$|\psi(t)\rangle = c_a(t)e^{-i\omega_a t}|a\rangle + c_c(t)e^{-i\omega_c t}|c\rangle + c_b(t)e^{-i\omega_b t}|b\rangle \tag{2.47}$$

Using the Schrödinger equation, with the interaction Hamiltonian:

$$H = \hbar\omega_a|a\rangle\langle a| + \hbar\omega_c|c\rangle\langle c| + \hbar\omega_b|b\rangle\langle b| - \frac{\hbar}{2}(\Omega_d e^{-i\phi_d}e^{-iv_d t}|a\rangle\langle c| + \Omega_p e^{-i\phi_p}e^{-iv_p t}|a\rangle\langle b|) + H.c. \tag{2.48}$$

the equations for the probability amplitudes can be derived as:

$$\dot{c_a} = \frac{i}{2}(\Omega_d e^{-i\phi_d}c_a + \Omega_p e^{-i\phi_p}c_b) \tag{2.49}$$

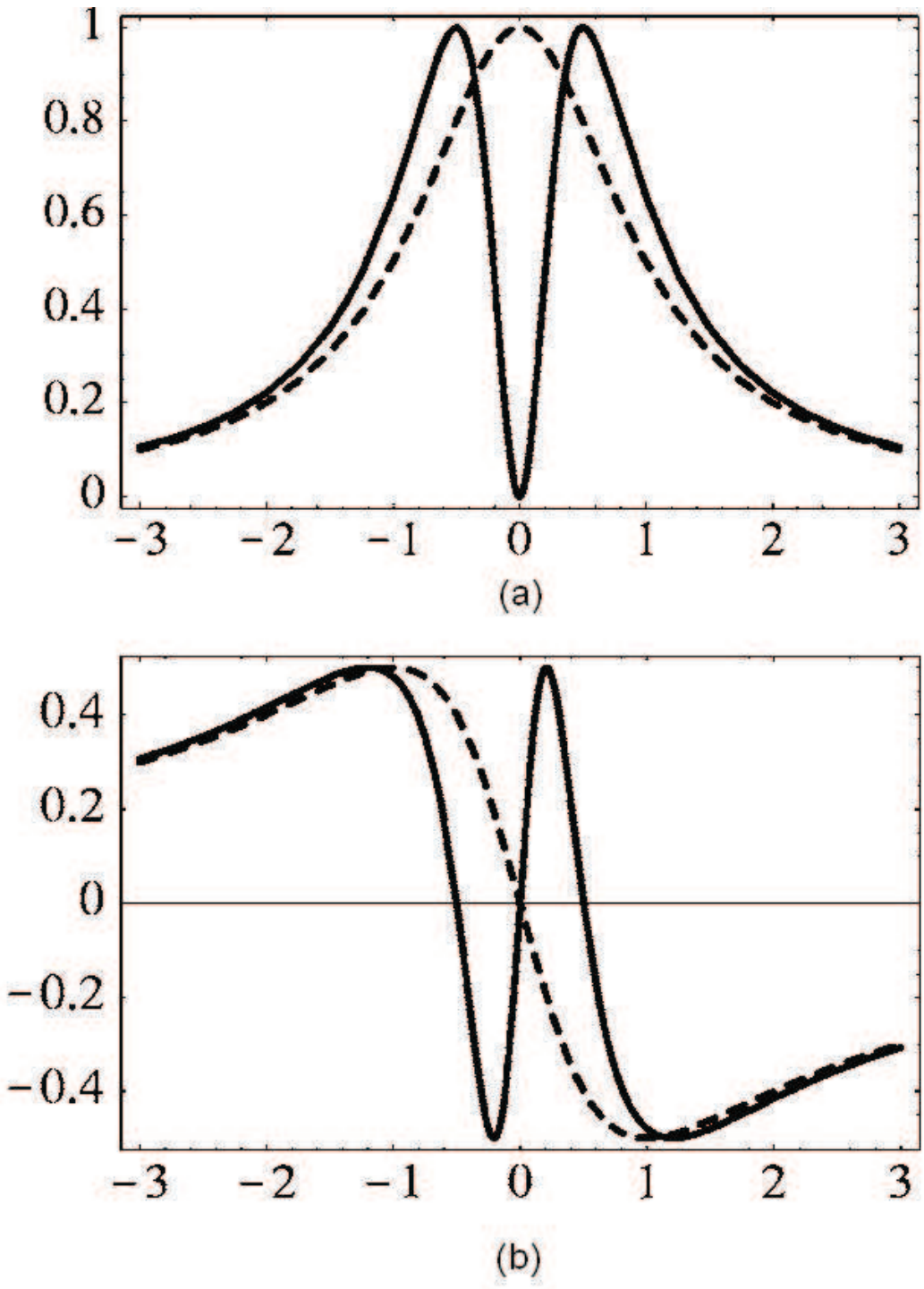

Fig. 4. Linear susceptibilities as the function of the detuning of the probe field: (a)imaginary part of susceptibility (b)real part of susceptibility. Dashed lines are for two level system and solid lines are for EIT system with resonant coupling field.[picture adopted from [33]]

$$\dot{c_c} = \frac{i}{2} e^{i\phi_d} \Omega_d c_a \tag{2.50}$$

$$\dot{c_b} = \frac{i}{2} e^{i\phi_p} \Omega_p c_a \tag{2.51}$$

If the atom is put into one superposition of the two lower states $|c\rangle$ and $|b\rangle$,

$$|\psi(0)\rangle = \cos(\theta/2)|c\rangle + \sin(\theta/2)e^{-i\psi}|b\rangle \tag{2.52}$$

and under the conditions:

$$\Omega_d = \Omega_p, \qquad \theta = \pi/2, \qquad \phi_1 - \phi_2 - \psi = \pm\pi \tag{2.53}$$

The equation of motion for the probability amplitude $c_1(t)$ remains close to zero, which means there is no absorption in the presence of both fields. We call the superposition of the two lower energy levels the dark state. There are many ways to evolve into the dark state, such as adiabatic population transfer. The shape of EIT resonance is described as a Lorentzian with full width at half maximum(FWHM):

$$\Gamma_{EIT} = 2(\gamma_{bc} + \frac{|\Omega_d|^2}{\gamma}) \tag{2.54}$$

However, if the probe field is not weak enough, with the situation $\gamma_{cb} \ll |\Omega_p|^2/\gamma \ll |\Omega_d|^2/\gamma$, we need keep the probe in our equations, which complicates the analytical solution. However, we could use a numerical solution of density matrix equations [34]. The real part of the susceptibility is responsible for the phase change of the electromagnetic field which is connected to the index of refraction:

$$n = 1 + \frac{\chi'}{2} \tag{2.55}$$

The index of refraction is crucial for the explanation of slow light experiments.

Usually, when we are studying light interacting with moving atoms we need consider the Doppler shift in the real experiments. The whole ensemble of moving

atoms with thermal distribution can be written as:

$$M_u(v) = \frac{1}{\sqrt{\pi}u} e^{-\frac{v^2}{u^2}} \tag{2.56}$$

Therefore,

$$\chi = \int_{-\infty}^{\infty} \chi(v) M_u(v) dv \tag{2.57}$$

where $u = \sqrt{2k_bT/m}$, T is the temperature of the medium. For a weak probe and $\Delta = 0$, the width of the EIT resonance is [35] [36]:

$$\Gamma_{EIT} = \begin{cases} \sqrt{\frac{2\gamma_{bc}}{\gamma}\Omega_d} & \text{if } x \ll 1; \\ \frac{|\Omega_d|^2}{W_D} & \text{if } x \gg 1. \end{cases} \tag{2.58}$$

where W_D is the width of the thermal distribution, and

$$x = \frac{|\Omega_d|^2 \gamma}{2\gamma_{bc} W_D^2}$$

when EIT occurs, and the upper state probability amplitude remains close to zero, gain can be present without the requirement of population inversion. This is an example of amplification without inversion. There are also spectral regions for which the refractive index is very high while the absorption vanishes. A change in absorption (or gain) over a narrow spectral range is accompanied by a change in refractive index over a similarly narrow region. As shown in the next section, this rapid change in refractive index produces an extremely low group velocity.

B. Slow light

The group velocity of light in media can be written as:

$$v_g = \frac{d\omega}{dk} \tag{2.59}$$

And as we all know, the spatial dispersion is:

$$ck = \omega n(\omega, k) \tag{2.60}$$

Therefore,

$$c = \frac{d\omega}{dk}n + \omega\frac{\partial n}{\partial \omega}\frac{d\omega}{dk} + \omega\frac{\partial n}{\partial k} \Rightarrow c = v_g(n + \omega\frac{\partial n}{\partial \omega}) + \omega\frac{\partial n}{\partial k} \tag{2.61}$$

where,

$$v_g = \frac{d\omega}{dk} = \frac{c - \omega\frac{\partial n(\omega,k)}{\partial k}}{n(\omega, k) + \omega\frac{\partial n(\omega,k)}{\partial \omega}} \tag{2.62}$$

For dispersionless media, $n(\omega, k) = n$, $V_g = c/n$. However, for media with frequency dispersion $n(\omega, k) = n(\omega)$, the group velocity is

$$v_g = \frac{c}{n + \omega\frac{\partial n}{\partial \omega}}$$

The group velocity of light can be reduced to several hundreds meters per second or even less because of the steep frequency dispersion associated with the narrow EIT resonance. This was first found by Harris' group [17], in which they found that when the absorption is swept through zero, the refractive index varies rapidly which means a significantly reduced group velocity.

The first experiment showing ultra-slow light was demonstrated by Hau group [20], which used EIT a Lambda scheme in a sodium Bose-Einstein condensate. The Hau group reported group velocities as low as 17 ms^{-1}. And slow light was also demonstrated in hot media. Kash et al. [18] performed slow light experiment in rubidium vapor at about $360K$ using EIT with Lambda scheme. By carefully choice of the experimental parameters, group velocity of 90 ms^{-1} was demonstrated. Also they showed that the Doppler free configuration is not necessary for observing slow light. Further slow light 8 ms^{-1} was demonstrated in hot gas again by Budker et al [22] in rubidium media, using different polarization of light and Zeeman sublevels. That group noted that the nonlinear magneto-optical effect is related to EIT with a group

delay. In a dense Doppler broadened medium, it is possible to obtain slow light close to zero group velocity. But under non-ideal conditions, the dark resonance decays due to the various dephasing mechanisms. There are many ways to increase the ground state coherence lifetime. For media with moving atoms, the coherence lifetime is limited by the interaction time of the atoms with the laser fields. Two common ways to increase the coherence of life time are the introduction of a buffer gas to confine the atoms [14] [37] [38], and by coating the cell walls [39] [40].

The nearly lossless slow propagation inside a medium is associated with many effects. The pulse can be spatially compressed because when the pulse enters the medium its front end propagates slower than its tail end by the ratio of slow group velocity to the speed of light [20]. Also due to the low loss of the electromagnetic field inside the medium and spatial compression of the field, the combination of atoms and coupling field store the electromagnetic energy.

Slow light remains the most exciting development along with EIT even years after the original idea was proposed. New ideas and new concepts are still appearing and new uses are still waiting to be made of them.

CHAPTER III

MODE-LOCKED RUBIDIUM LASER AND ITS COHERENT APPLICATIONS

A. Introduction

Laser (Light Amplification by stimulated Emission of Radiation) is the descendant of Maser (Microwave Amplification by Stimulated Emission of Radiation). The difference between these two is the range of the output frequency. The laser is based on the phenomenon of stimulated emission which gives laser light its coherence. Laser output can maintain its highly collimated direction, polarization. Laser media can be gas, semiconductor, liquid, solid. The output of a laser may be continuous wave and pulsed wave by using modelocking, Q-swithching or gain-switching techniques.

The first laser was obtained in solid ruby in 1960 [41] and one year later in helium-neon gas in 1961. Coherent radiation at various frequencies produced by lasers [42] [43] is used by many spectroscopic methods that have broad range of applications to biology, chemistry, and physics [44]. Development of new lasers as well as new regimes of laser operation is a continuous challenge for researchers. Recently, a new type of atomic laser system was proposed by Krupke et al [45]. The active medium for this type of laser is Rubidium atomic vapor. Energy levels of Rubidium atom are shown in Fig. 5. Lasing occurs on the excited $P_{1/2}$ to ground $S_{1/2}$ transition (the D1 line). To create a population inversion at this transition, a cell with a large density of a buffer gas, a mixture of helium and ethane is used. Atomic population excited by a diode laser (pump field) tuned to D_2 line populates the $^2P_{3/2}$, and then, the population is transferred to $^2P_{1/2}$ via collisions with the buffer gas. Similar lasers using other alkali atoms have also been studied by several groups of researchers [46] [47].

Inside the laser cavity, the light wave bounces between mirrors constructively forming a standing wave. The finite bandwidth of the laser output is determined by

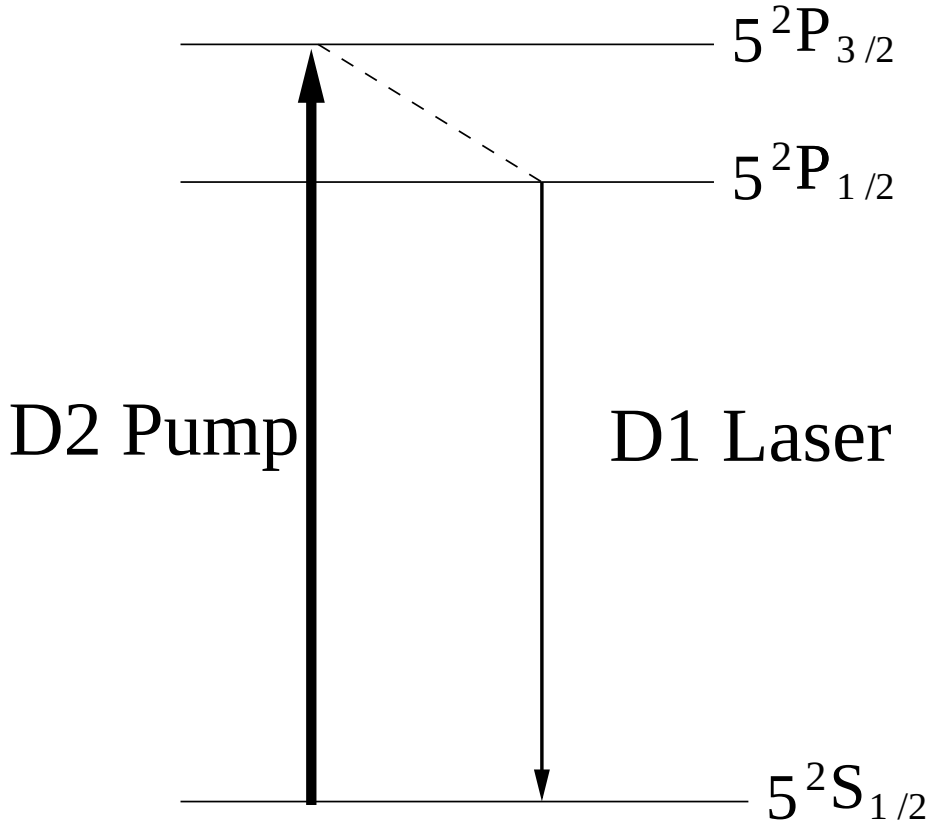

Fig. 5. Relevant energy levels of the Rubidium atom. D1 and D2 lines are dipole-allowed transitions, and the dotted line is the collisions mixing of fine structures [45].

the gain medium. The standing waves which can fit into the laser cavity are called longitudinal modes, mode spacing $\delta f = c/2L$, where L is the length of the cavity. Usually several cavity modes occur in the bandwidth of the lasing transition. When more than one longitudinal mode is excited, the laser is called a multi-mode laser. With independently oscillating modes, the phase of the modes is random with respect to each other, which leads to fluctuations in intensity. There are two methods to lock multi-mode lasers: active mode-locking and passive mode-locking. In this study, we achieve mode-locking by using active mode-locking. This is done by placing a frequency modulator into the laser cavity, and choosing a modulation frequency equal to the cavity mode spacing δf.

Coherent applications are demonstrated by carefully choosing the cavity length in order that an integer number of mode spacings is just equal to the ground state hyperfine splitting, then hyperfine coherence can be excited by these two different laser modes. In this way, the rubidium laser can be used as a useful tool for several spectroscopic applications. An EIT resonance can be observed in a Λ system consisting of two Zeeman sublevels of ground $5^2S_{1/2}$ state Rubidium atom as shown in Fig. 10 by coupling two orthogonal circular polarization components from two different laser modes. This is similar to the work by Sautekov et.al [48] and Arissian et.al [49] where EIT effects are observed by using mode-locked laser fields.

B. Experimental setup

A schematic of the experimental setup is shown in Fig. 6. An external-cavity diode laser system (Toptica DLX 110 laser system) tuned to the rubidium D2 transition is used as the pumping source. After an isolator, a polarization beam splitter is used to couple a linearly polarized continuous wave laser pump field into the laser cavity, and also to separate the D1 output laser field from the pump laser field. The gain medium is a 2.5 cm long cell containing a natural isotopic rubidium mixture together

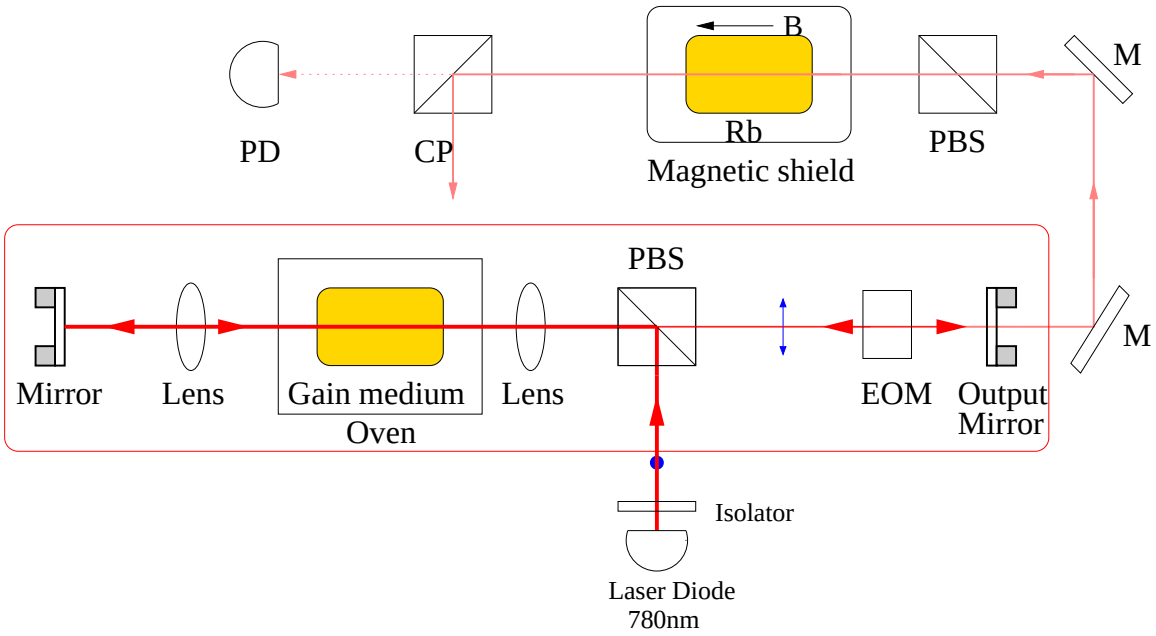

Fig. 6. Schematic diagram of the mode-locked rubidium laser and setup of the EIT and nonlinear Faraday effect experiments. PBS: Polarization Beam Splitter. EOM: Electro-Optical Modulator. CP: Cross Polarizer. PD: Photodetector.

with 525 torr of helium buffer gas and 75 torr of ethane [45]. The cell is heated to about 80°C in an oven with anti-reflection coated windows. The length of the laser cavity is chosen to be 3 meters to give a mode spacing of approximately 50 MHz. The pump laser was focussed into 500 μm diameter at the center of gain medium, producing a pump intensity of about 200 W/cm^2. A 30% reflectivity flat mirror is used as a laser cavity output coupler.

Fig. 7 shows the output power as function of the amount of pump power absorbed by the gain medium at a density of rubidium atoms of 8.2×10^{11} cm^{-3}. Laser power efficiency of 16.7% is achieved and the laser threshold is about 120.8 mW.

The output laser field is detected and monitored by a spectrum analyzer. To achieve active mode locking, an electro-optic modulator (EOM) is placed inside laser cavity with modulation frequency near cavity mode spacing $\Delta v = c/2L = 55$ MHz.

For our coherence applications, the linearly polarized Rb laser output is sent into another Rb cell with a natural mixture of ^{87}Rb and ^{85}Rb. A three-layer magnetic shield

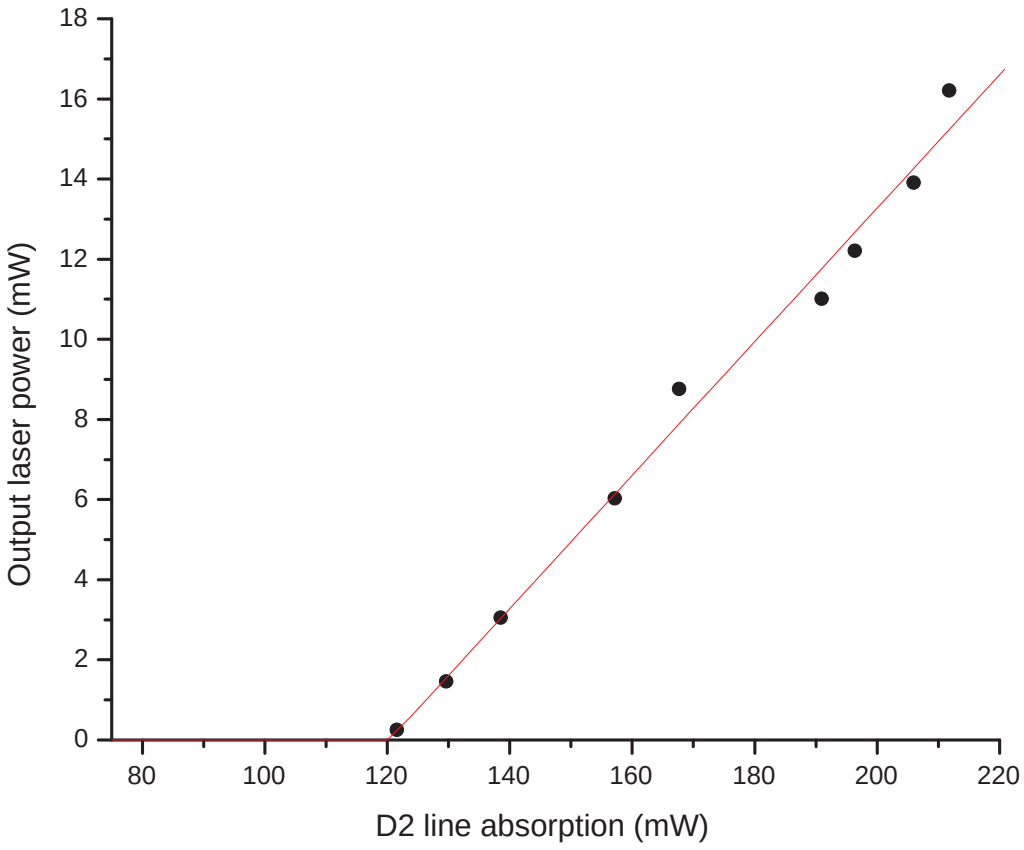

Fig. 7. Laser output power versus the pump source input power at a rubidium density of 8.2×10^{11} cm^{-3}.

is used to reduce the stray magnetic field in the cell. The rubidium cell is not heated during these measurements. Two solenoids are used to supply a varying magnetic field: one provides a large Zeeman splitting of the Rb ground state, and another is used to scan the magnetic field in a small range. Transmission of the field through the cell is detected after a crossed polarizer. The EIT resonance is observed when the Zeeman splitting matches the frequency separation of two adjacent laser modes. The nonlinear Faraday effect is also observed by scanning the magnetic field in small range. Two orthogonal circular polarization components from the same longitudinal mode couple with Zeeman sublevels. Due to the steep dispersion, the refractive indexes changes rapidly as the Zeeman sublevels shift. The difference between the optical phase acquired by different circularly polarized components travelling through a resonant medium results in rotation of the transmitted linear polarization of the light field.

C. Mode-locked rubidium laser

Before the frequency modulator is put inside the laser cavity, the laser operation is continuous wave (cw) with the different modes oscillating independently. There are many methods to force each mode to operate with a fixed phase relationship, falling into two categories: active mode locking is when external signals to modulate the field inside the laser cavity, for example acoustic-optic or frequency modulators inside the laser cavity, with modulation equal to the cavity mode spacing Δf, can result in active mode locking. Passive mode locking involves changing the intracavity elements to produce self-modulation of the light, such as by using a saturable absorber inside the cavity.

By applying these methods, the laser output behaves differently compared to cw laser operation. Mode-locked lasers produce pulses of light separated in time by $t = 2L/c$, where t is the time for light to travel one round trip inside the laser cavity

and $t = 1/\Delta f$. The width of laser pulse is determined by the number of modes which are locked. Theoretically, the more modes are locked, the shorter the pulse duration will be. But in the real experiments, the pulse duration also depends on other effects.

In this study, a frequency modulator is used to achieve active mode locking of the rubidium laser. The frequency modulator induces a sinusoidally varying frequency shift in the light passing through it. In the frequency domain, the modulation of the light results in optical sideband frequencies, separated by the modulation frequency. If the modulation frequency is equal to the cavity mode spacing, the sidebands can connect two cavity modes adjacent to the central optical frequency. Those sidebands are in phase with the central optical mode, which induces a definite phase relationship between the central mode and the adjacent modes. In this way, all modes inside the gain bandwidth can be phase locked to produce a short pulse of light.

For our rubidium laser operating on the rubidium D1 transition, the large amount of helium buffer gas produces a collisional broadening of 6.2 GHz. With a cavity mode spacing $\Delta f = c/2L \cong 55$ MHz at cavity length of 3 meters , as many as 110 different modes can be oscillating simultaneously, and can compete with each other inside this cavity. In addition, the amplitude and phase of each mode could be changing with time in a completely uncorrelated way. To achieve mode locking, we inserted an EOM inside the the laser cavity. A sinusoidally varying electrical signal induces a time-varying phase to the fields passing through the cavity. By matching the frequency of modulation to the cavity mode spacing, phases of different modes are forced into definite phase relationship. Fig. 9 shows the beating signal after mode-locking method with modulation frequency $f = 55.3309$ MHz, compared with beating signal without mode locking Fig. 8. We observe a narrow beat signal after the cavity modes are locked. The full-width at half maximum (FWHM) linewidth of the beat note between longitudinal modes can only be measured to be less than 2 kHz due to the limit of the spectrum analyzer we used.

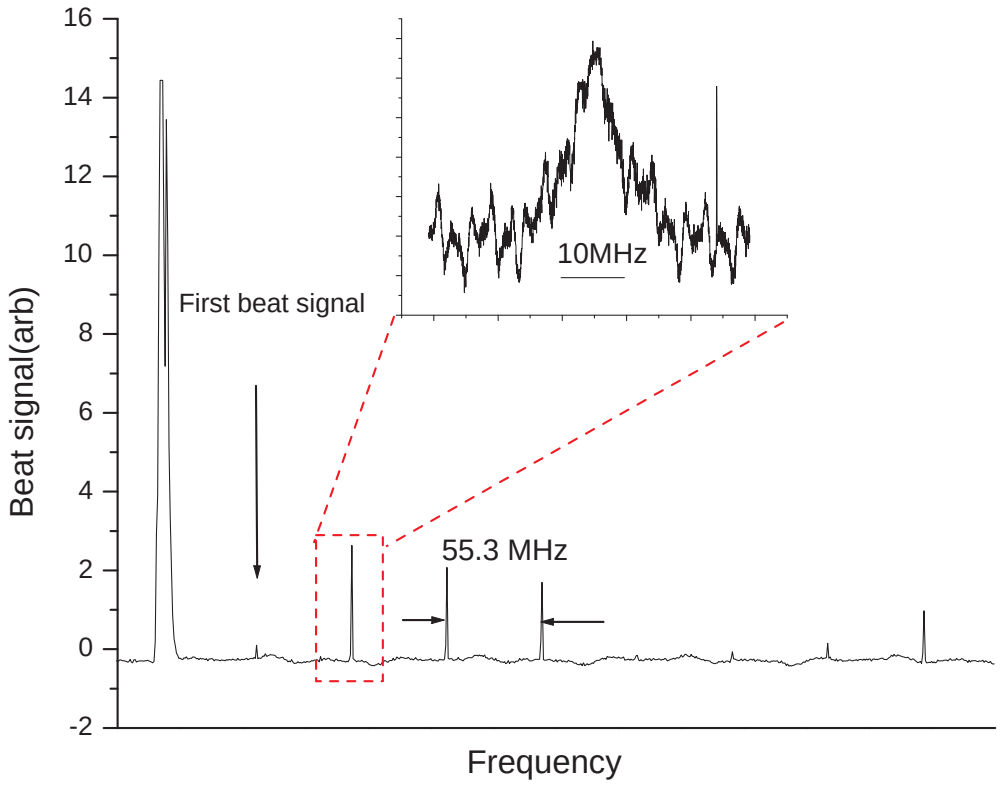

Fig. 8. Beating signal of different modes from multi-mode Rubidium laser output without mode-locking.

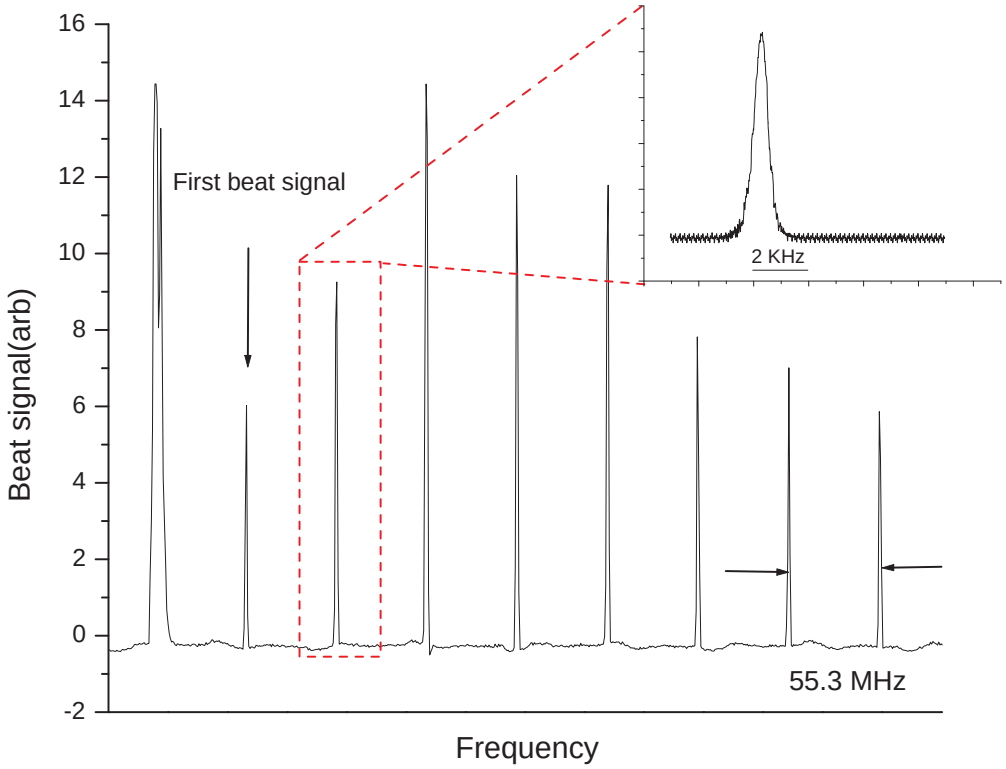

Fig. 9. Beating signal of different modes from multi-mode Rubidium laser output with mode-locking.

D. Coherent effects by mode-locked rubidium laser output

Due to the narrow beating signals from our mode-locked rubidium laser, EIT resonance can be observed in a Λ system consisting of two Zeeman sublevels of the ground $5^2S_{1/2}$ state of rubidium as shown in Fig. 10. Linearly polarized output from the rubidium laser can be considered as two equal amplitude opposite circular polarization components, which couple to different Zeeman sublevels. Therefore, two orthogonal circular polarization components from two different laser modes can create a coherent superposition in Zeeman sublevels when a longitudinal magnetic field is applied.

For the ^{85}Rb atom, the Zeeman splitting for the ground state $v_z = K_z B$ can be calculated to be $K_z = 466.74$ kHz/G. When the Zeeman splitting for the ground state is about $v_z = 55.3$ MHz after applying a large longitudinal magnetic field through solenoids, EIT resonance is observed. This is shown in Fig. 11 with some linear Faraday effect background [50].

Another coherent effect: nonlinear magneto-optic rotation (nonlinear Faraday effect) [22][51] has also been observed using our mode-locked laser system. By scanning the magnetic field in a small range, we observe the nonlinear Faraday effect near zero magnetic field. The result is shown in Fig.12. In this scheme, two orthogonal circular polarization components from same longitudinal mode couple two degenerate Zeeman sublevels at zero magnetic field, constituting a simple Λ system.

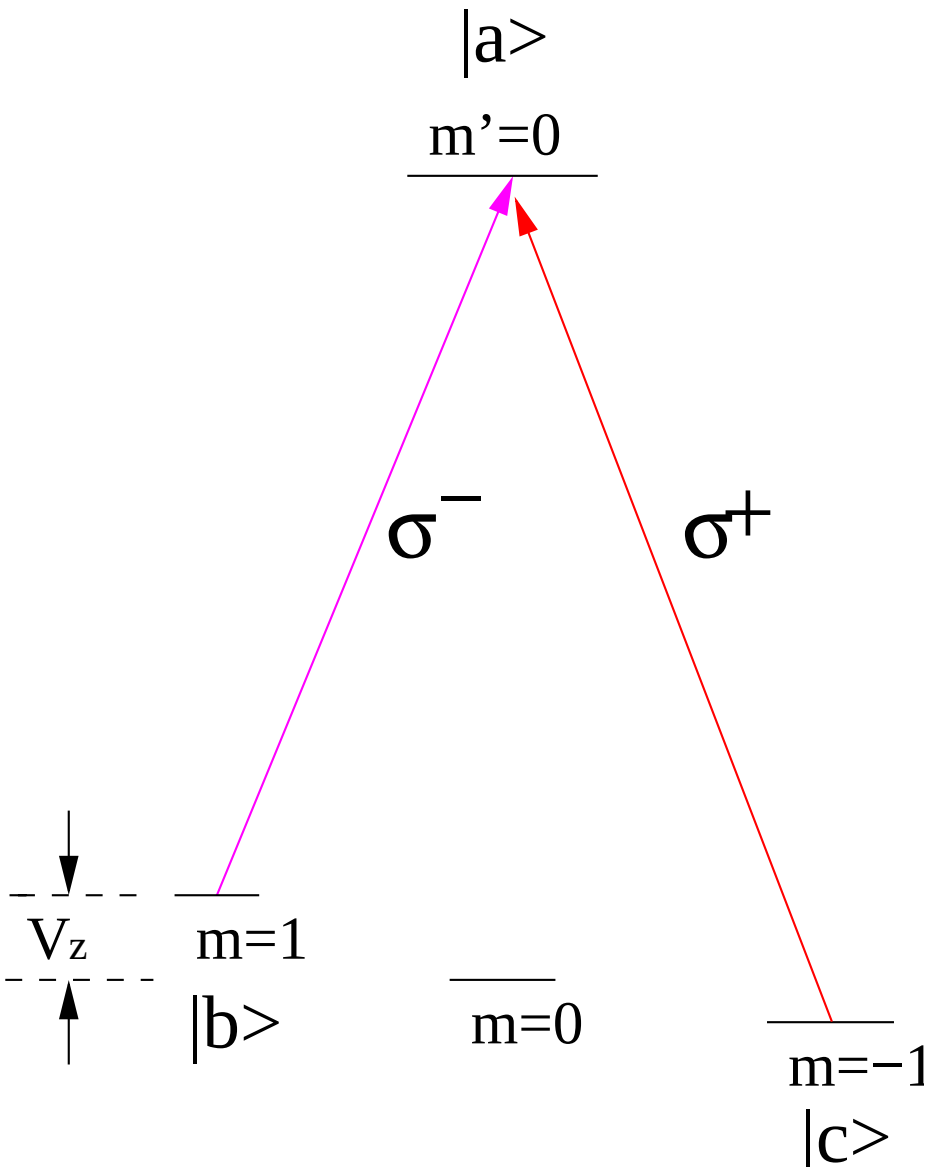

Fig. 10. EIT in Λ Configuration of ^{85}Rubidium energy level at transition $(5^2S_{1/2}(F = 3) \rightarrow 5^2P_{1/2}(F' = 3))$ with one excited level and two Zeeman sublevels of ground state. Two optical fields are composed of orthogonal circular polarizations from different modes.

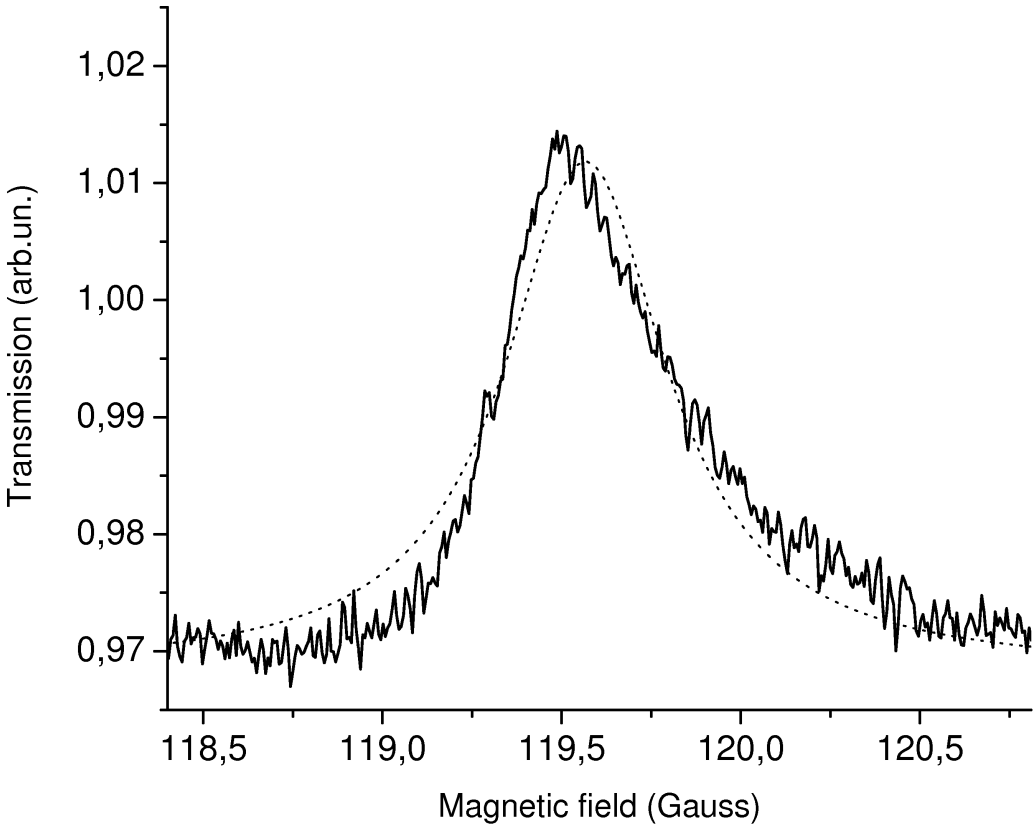

Fig. 11. When Zeeman splitting was tuned around $v_z = 55.8$ MHz,EIT coherent effect was observed.

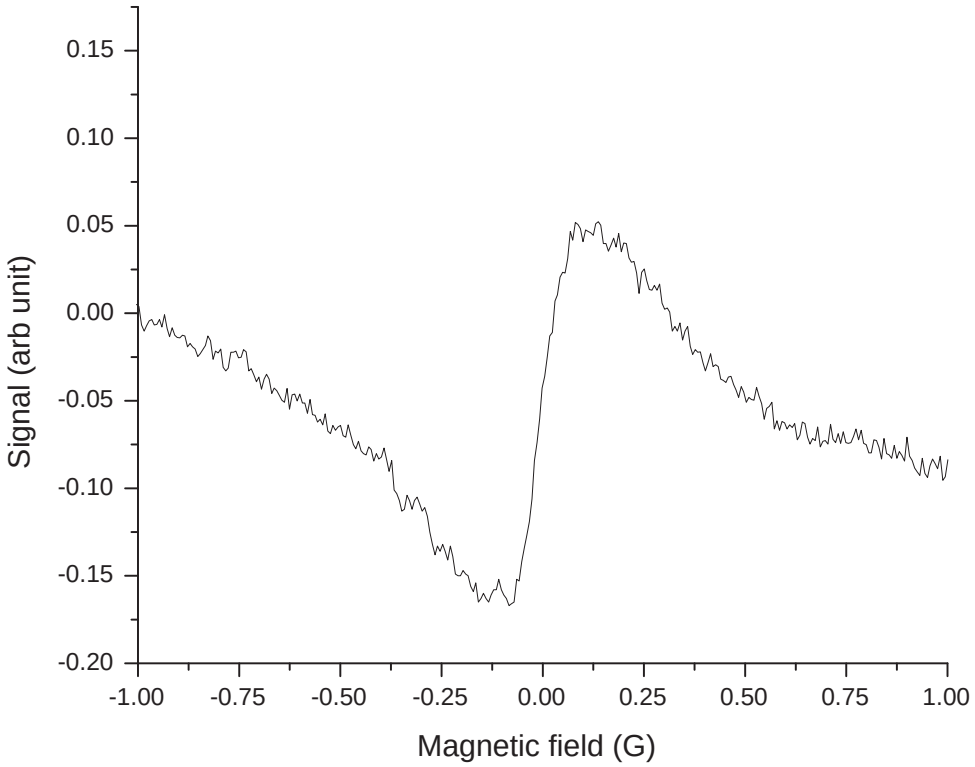

Fig. 12. Nonlinear Faraday effect by scanning magnetic field.

E. Discussion and summary

In our rubidium laser system gain medium, 525 torr buffer gas helium was used with a natural isotopic mixture of rubidium metal. Collisional broadening by buffer gas at 80°C in rubidium principal transition can be estimated 6.2 GHz [52]. With this amount of buffer gas, homogenous broadening from collisions is much larger than other broadenings, such as power broadening or Doppler broadening. Population inversion between the $5^2P_{1/2}$ state and $5^2S_{1/2}$ state can be easily achieved as long as a fast transfer rate between fine structure sublevels ($5^2P_{3/2} \rightarrow 5^2P_{1/2}$) can be obtained. This is the reason we also add the hydrocarbon molecule ethane to the gain medium. The population transfer for fine structures of alkali by adding hydrocarbons molecular had been investigated. [53] [54]. Seventy-five torr ethane included inside the gain medium will result in a fine structure mixing rate of rubidium ($5^2P_{3/2} \rightarrow 5^2P_{1/2}$) to 0.4 nsec, which is shorter than the lifetime 25.5 nsec lifetime of the 5^2P state. As a result of transition broadening by the buffer gas and fine structure mixing by molecular ethane, population inversion between the $5^2P_{1/2}$ and $5^2S_{1/2}$ states is obtained in this gain medium.

In this work, when the Zeeman splitting matched frequency difference between two modes, a coherent superposition between two lower states is achieved [55]. The width of the EIT resonance was measured to be about 300 kHz, which is smaller than the natural width of the rubidium optical transition 6 MHz. Recently, it was demonstrated that intensity correlations manifesting matched pulses under EIT conditions can smoothly switch to Raman anti-correlation by introducing a two-photon detuning [56] [57].

We also observed nonlinear Faraday effect by scanning the magnetic field near zero using the same setup. Due to the steep dispersion of EIT, refractive indexes change rapidly as the Zeeman sublevels shift. The difference between the optical phase acquired by two circularly polarized components traveling through the coherent

medium results in rotation of the laser field polarization. It is useful to study these phenomena with this laser, because it provides a system with low phase noise, and could lead to improvement of noise characteristics of laser systems.

In conclusion, we experimentally demonstrated mode-locked regime for the first time for this type of laser. A mode-locked rubidium laser was operated on the D1 transition. In this experiment, an EOM was introduced into the laser cavity to lock different cavity modes with modulation frequency equal to cavity mode separation. From the beat signal of different modes from the multimode laser output, we can easily recognize the onset of active mode-locking. This regime allows us to use such lasers to demonstrate quantum coherence effects, in particular, the EIT resonance and nonlinear Faraday effects. This three level end-pumped laser oscillator which is based on rubidium fine structure energy level population inversion has large gain for laser output.

CHAPTER IV

ENHANCED COUPLING BETWEEN OPTICAL AND SOUND WAVES IN FORWARD DIRECTION

A. Introduction and motivation

The narrow EIT resonance which is accompanied by steep dispersion leads to ultra-slow light. In 2001 Matsko et al. [58] described the phenomenon of forward stimulated Brillouin scattering (SBS). Due to the energy momentum conservation rule, forward stimulated Brillouin scattering is usually forbidden. SBS is normally associated with strong backward scattering. However, in ultra-dispersive coherent media, maximum scattering is along the forward direction instead of the backward direction. This gives promise to obtain effective squeezing [59].

Let us first study the properties of light scattering in the three-level Λ-type media. We will see that if the group velocity associated with EIT in the media matches the acoustic velocity, then SBS can be predicted, along with strong acousto-optical interaction.

Consider two coherent electromagnetic waves propagating in a dielectric medium in Λ-type EIT. A strong field of frequency ν_d is the coupling field and a weak field of frequency ν_1 is the probe field. Now, suppose the electromagnetic fields are propagating in the presence of an acoustic wave of frequency ω_b as shown in Fig. 13. Then the probe field ν_1 becomes modulated at the sound frequency while it propagates through the medium, resulting in a new field ν_2 where $\nu_2 = \nu_1 \pm \omega_b$. The amplitude of this modulation depends on the coupling between the optical and acoustic waves, and also depends on the direction of propagation of the waves.

The wave vector of the acoustic wave need to satisfy the momentum conservation rule:

$$\vec{k_2} - \vec{k_1} = \vec{q} \tag{4.1}$$

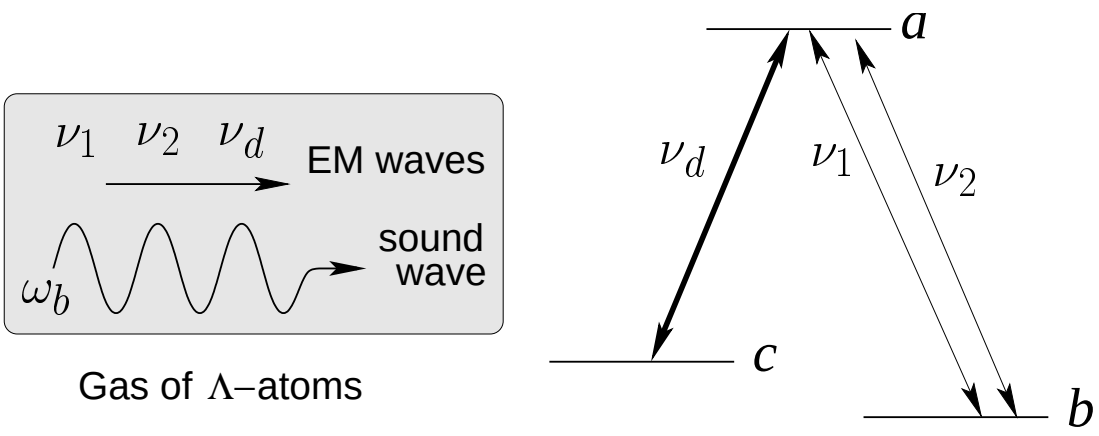

Fig. 13. Schematic of the acousto-optical interaction. Two probe electromagnetic fields with frequencies ν_1 and ν_2 and a coupling field with frequency ν_d propagate in a coherent medium consisting of three level atoms in which both probe fields are in approximate Λ configuration with the coupling field. A sound wave of frequency ω_b couples the two probe fields $\nu_{1,2}$.

Also, by the energy conservation rule,

$$v_1 - v_2 = \omega_b \tag{4.2}$$

Therefore,

$$|\vec{q}|^2 = |\vec{k_1}|^2 + |\vec{k_2}|^2 - 2|\vec{k_1}||\vec{k_2}|\cos\theta = (|\vec{k_1}| - |\vec{k_2}|)^2 + 4|\vec{k_1}||\vec{k_2}|\sin^2\frac{\theta}{2} \tag{4.3}$$

For the dipersionless medium, $|\vec{k_2}| \approx |\vec{k_1}| = vn/c$ and with

$$|\vec{q}| = \omega_b/V_s \tag{4.4}$$

where V_s is the speed of sound inside the media. We can easily get:

$$|\vec{q}| = 2\frac{vn}{c}\sin\frac{\theta}{2} \tag{4.5}$$

$$\omega_b = 2\frac{nV_s}{c}v\sin\frac{\theta}{2} \tag{4.6}$$

From above two equations, the SBS vanishes when $\theta = 0$. However, for the ultradispersion media [58],

$$|\vec{k_1}| - |\vec{k_2}| = \frac{v_1 n(v_1)}{c} - \frac{v_2 n(v_2)}{c} \approx \frac{v_1 - v_2}{c}\frac{\partial[vn(v)]}{\partial v} = \frac{v_1 - v_2}{V_g} \tag{4.7}$$

Therefore, we can rewrite:

$$|\vec{q}| = \sqrt{(\frac{\omega_b}{V_g})^2 + 4\frac{vn}{c}(\frac{vn}{c} - \frac{\omega_b}{V_g})sin^2\frac{\theta}{2}} \tag{4.8}$$

Combining the above equation and previous Equ.[4.5], we can get:

$$\omega_b^2\frac{V_g^2 - V_s^2}{4V_s^2V_g^2} - \frac{vn}{c}(\frac{vn}{c} - \frac{\omega_b}{V_g})sin^2\frac{\theta}{2} = 0 \tag{4.9}$$

This equation gives the acoustic frequency for backward scattering when $V_g \geq V_s$

$$\omega_b^b = 2\frac{nV_s}{c}v\frac{V_g}{V_g + V_s} \tag{4.10}$$

however for the forward scattering:

$$\omega_b^f \leq \frac{nV_s}{c}v \tag{4.11}$$

Thus, we see that when the group velocity of the light field is equal to the acoustic velocity, forward scattering is strongly allowed while the backward scattering is forbidden.

B. Experimental setup

The experimental setup is shown schematically in Fig. 14. An external cavity diode laser is tuned to the vicinity of the $5S_{1/2}F = 2 \rightarrow 5P_{1/2}F' = 2$ transition of Rb (the D_1 line). This laser is referred to as the coupling field (ν_d) in Fig. 13. Sidebands are generated on the coupling laser by an electro-optic modulator (EOM) which is tunable to the vicinity of the 6.835 GHz ground state splitting [18], so that the high frequency sideband serves as the probe field (ν_1) driving the $F = 1 \rightarrow F' = 2$ transition. The

power of the sideband can be changed by changing the EOM driving power. However, a disadvantage of this setup is that we can not suppress the Stokes component of the field. Fortunately, this lower frequency sideband is far off resonance, and has only a negligible effect on the experiment. After the EOM, all fields pass through a single-mode optical fiber to obtain a clean Gaussian spatial mode. The laser is collimated to a diameter of 4 mm, and circularly polarized with a $\lambda/4$ wave-plate just before the cell. The cell is 2cm long and contains Rb and 3 torr neon buffer gas. It is installed in a 3 layer magnetic shield which suppresses the laboratory magnetic field. The cell is heated to 60-70°C to control the density of Rb vapor.

Before the EOM, part of the coupling laser is split from the main beam, shifted in frequency by a small amount (60 MHz) with an acousto-optic modulator and deflected around the cell. This shifted beam is recombined with the light transmitted through the cell, and all the fields are detected on a fast photodiode and monitored by the spectrum analyzer. Since the photo current contains beat signals at various RF frequencies which are combinations of the 60 MHz shift and the $6,835$ GHz separation of the probe and drive fields. These components can be isolated with a spectrum analyzer, allowing us to distinguish the transmitted probe and Stokes component of the field. This (heterodyne) procedure is discussed for a similar setup in Ref. [18].

A sound wave with frequency 1.5 kHz is generated in the cell by using piezoelectric activators. The sound wave is created in the cell by modulating a the piezo-electric device which is bonded to the surface of Rb cell. We apply a sinusoidal voltage to piezo which results in a sinusoidal displacement of the cell, which behaves like a diaphragm and generates a traveling acoustic wave inside the cell. The maximum displacement amplitude created by the piezo at the end of cell is about 3μm. The speed of sound in the neon buffer gas is 482 m/s at the temperature of 65.0°C.

The group velocity is measured as in Ref. [18]. By modulating the intensity of the probe field before the cell, the time delay is observed in the transmitted probe field.

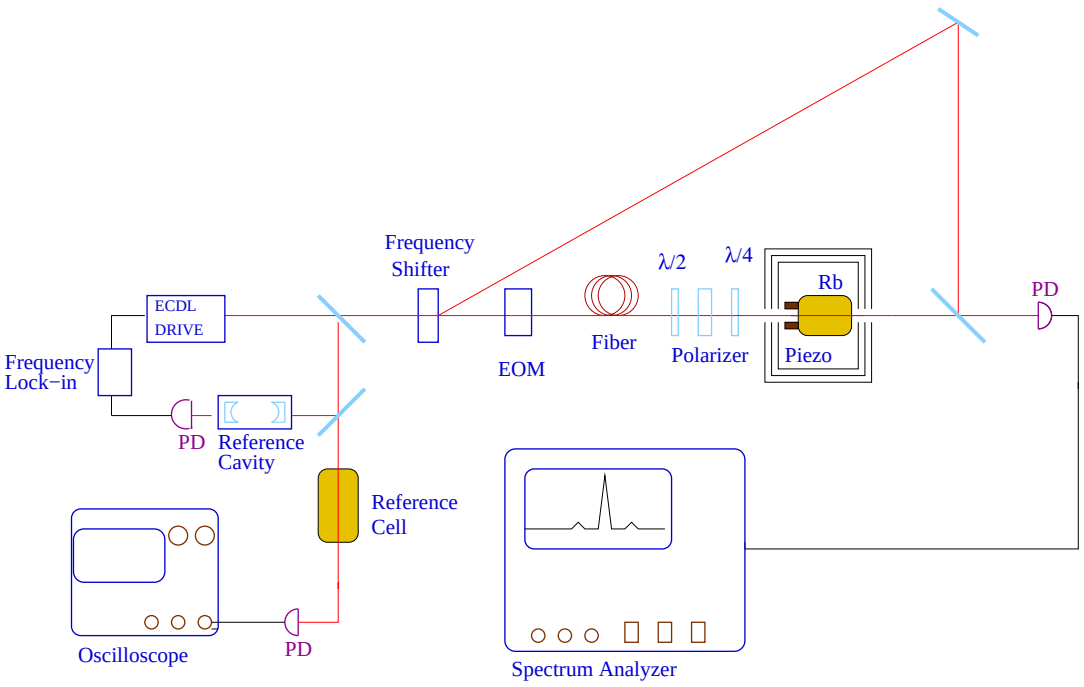

Fig. 14. Experimental setup.

In this experiment, we use a sinusoidal modulation of the probe field amplitude. By using lock in detection of the transmitted probe field, the time delay can be precisely measured [71]. With this method, we measure the phase shift between the transmitted and bypassed probe fields. For sinusoidal modulation, this phase shift can be written as [71]:

$$\psi = 2\pi t_a f - \psi_0 \tag{4.12}$$

where t_a is the time delay due to the reduced group velocity by the Rb atoms, and ψ_0 is a constant phase shift. By measuring the phase shift versus modulation frequencies, the constant phase shift can be eliminated, and the slope is $2\pi t_a$. The group velocity is then just given by $v_g = L/t_a$ for a cell of length L.

C. Experimental results

An important result of this section is shown in Fig. 15. This shows the spectrum of the probe field after propagating through the cell for two cases of the group velocity.

In the first case (a) the spectrum of the probe field is shown when the group velocity of the light is of the order of the velocity of sound. In this case, sidebands are observed at the sound frequency with about 20% of the energy of the central peak. In case (b) the group velocity is far higher than the velocity of sound and no side bands are observed. Experimentally, the difference between these two cases is the temperature of the cell (and so the density of rubidium atoms), which demonstrates that the modulation of the probe field is not taking place in the glass, optics, or due to other systematic errors.

We have measured the group velocity as a function of coupling laser power and found the expected linear relationship as shown in Fig. 16. Correspondingly, the width of the EIT resonance (FWHM) increases with optical power as shown in Fig. 17. We have also measured the ratio of the acoustically generated sideband intensities to the probe intensity as a function of laser power. Using these two results, we can plot the ratio of the acoustically generated sideband intensity as a function of group velocity. This is shown in Fig. 18. It is easy to see that there is a maximum of the intensity of the sidebands, and the maximum corresponds to the group velocity of light being of the order of the velocity of sound.

We note that low group velocity corresponds to low coupling laser power. As the coupling power is decreased, the EIT resonance linewidth decreases, and absorption of the sidebands becomes a problem when the EIT resonance half-width falls below the sideband separation (i.e., the sound frequency). In the experiment, the sound frequency is 1.5 kHz and the measured EIT linewidth is 3.0 kHz for a coupling laser power corresponding to a group velocity of about 170 ms^{-1}. This is seen in the figure as the point at which maximum side-band intensity is recorded.

We also studied the generated sideband intensities and group velocity as function of with one photon detuning and two photon detuning. Fig. 19 shows the generated sideband intensities related to the one photon detuning. Fig. 20 gives the generated

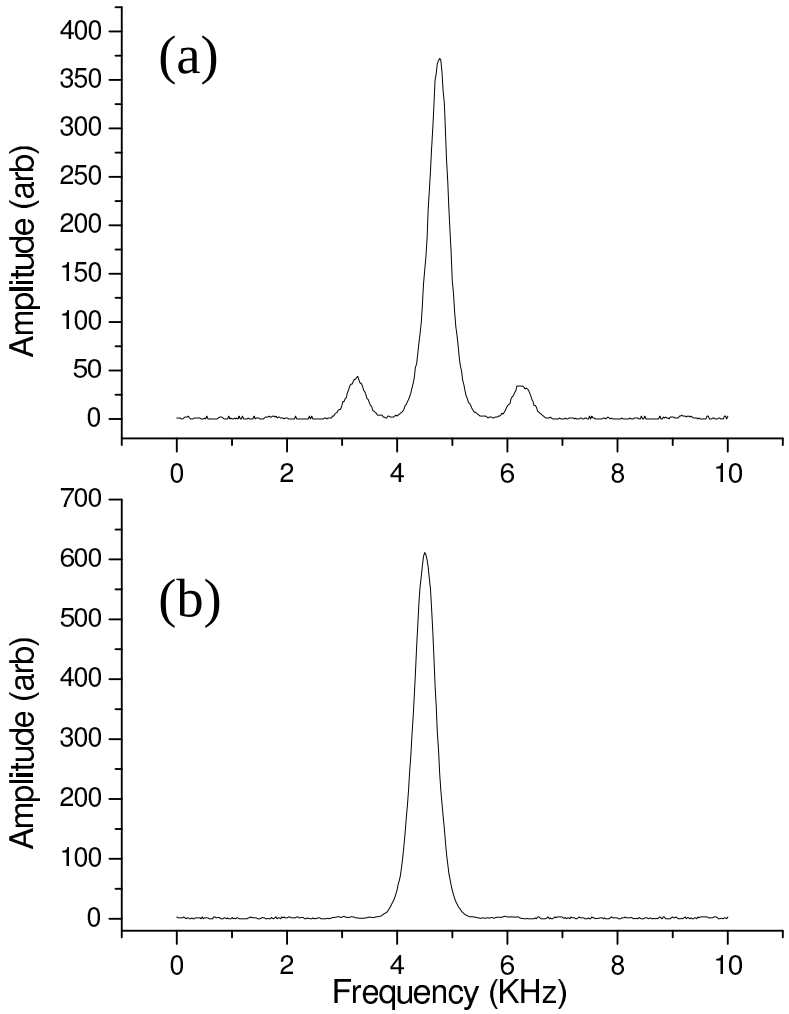

Fig. 15. (a) The spectrum of the probe field in the case where the group velocity of light is approximately equal to speed of the sound wave. The cell temperature is 66.4° C, and the density of ^{87}Rb is 1.2×10^{11} cm^{-3}. (b) The spectrum of the probe field in the case where the group velocity of light is very different from the speed of the sound wave. The cell temperature was 25° C and the Rb vapor density is too low to significantly affect the group velocity. In both cases the sound wave frequency is 1.5 kHz. The total optical power before the cell was 320 μW and the group velocity of the probe light in this case (a) is 480 m/s.

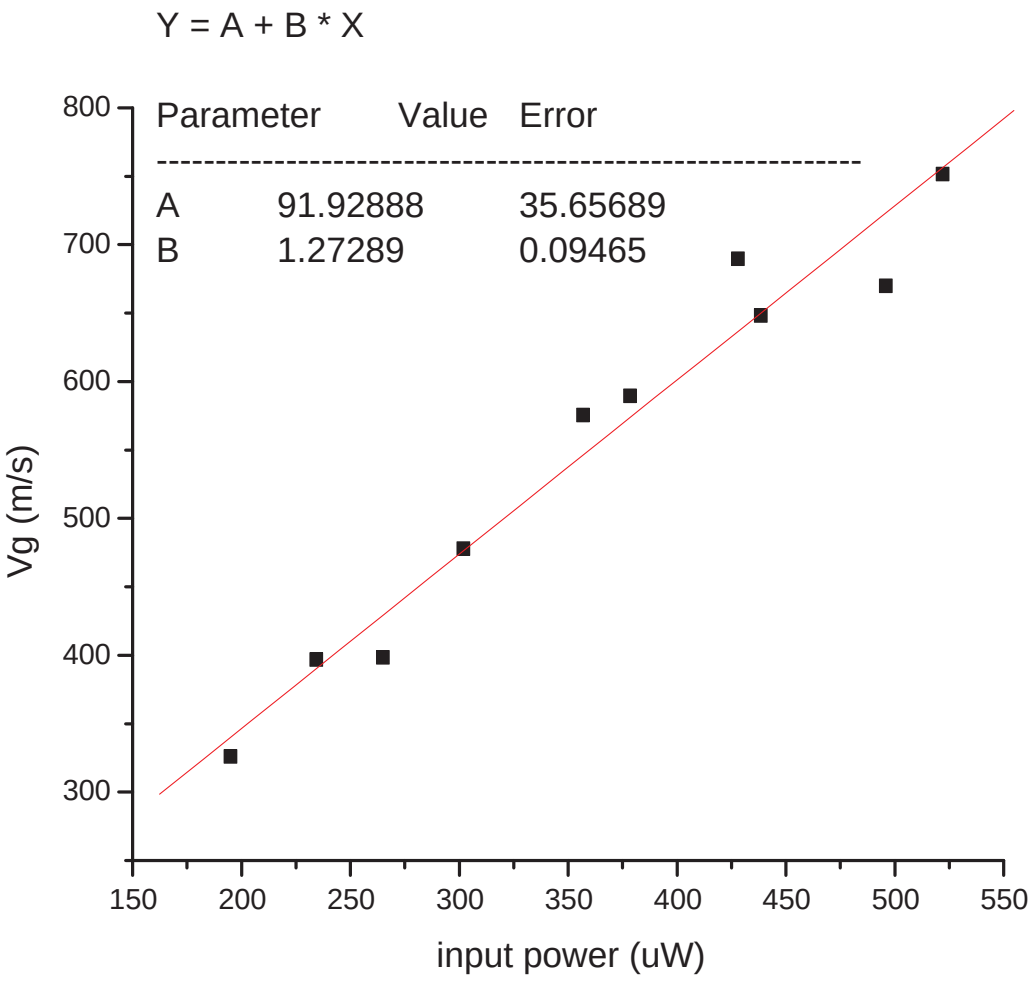

Fig. 16. Dependence of group velocity with the power of transmitting laser field after the cell at the temperature at 65.0°C, with the density of Rb atom $1.1 \times 10^{11}[1/\mathrm{cm}^3]$.

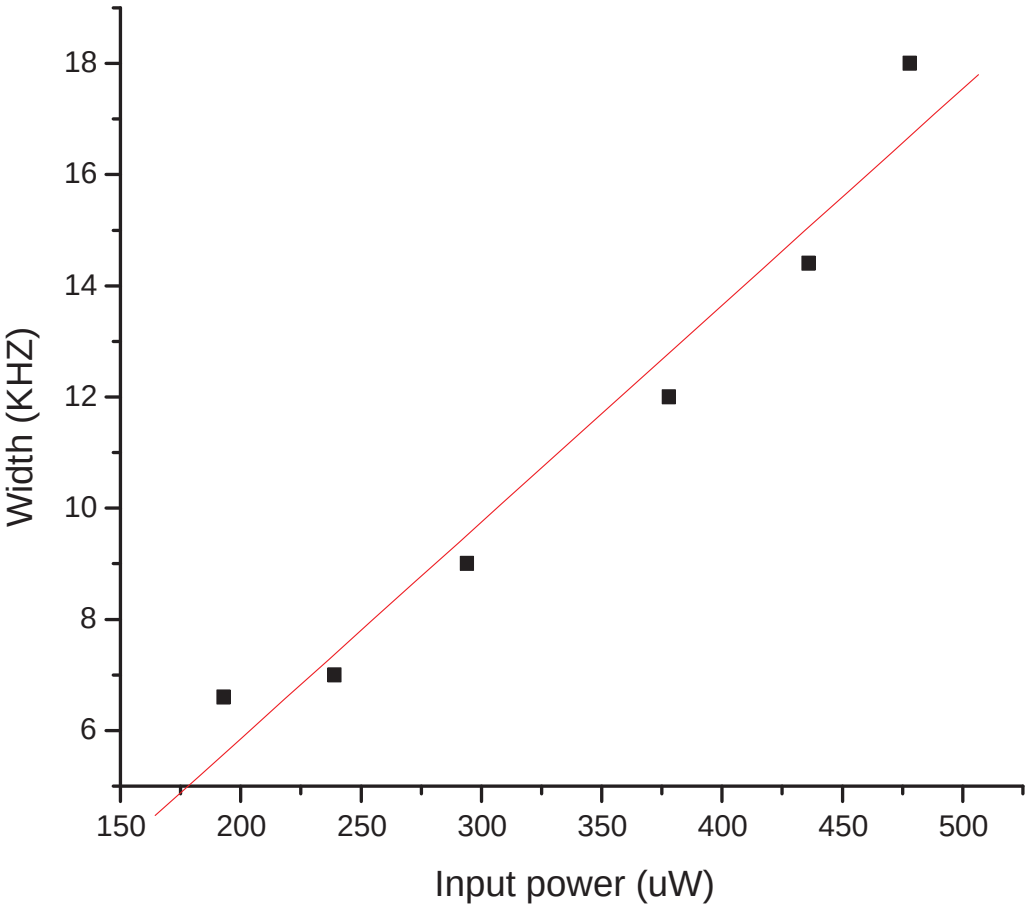

Fig. 17. Dependence of the width of EIT resonance (FWHM) with the power of transmitting laser field after the cell at the temperature at 65.0°C, with the density of Rb atom $1.1 \times 10^{11}[1/\mathrm{cm}^3]$.

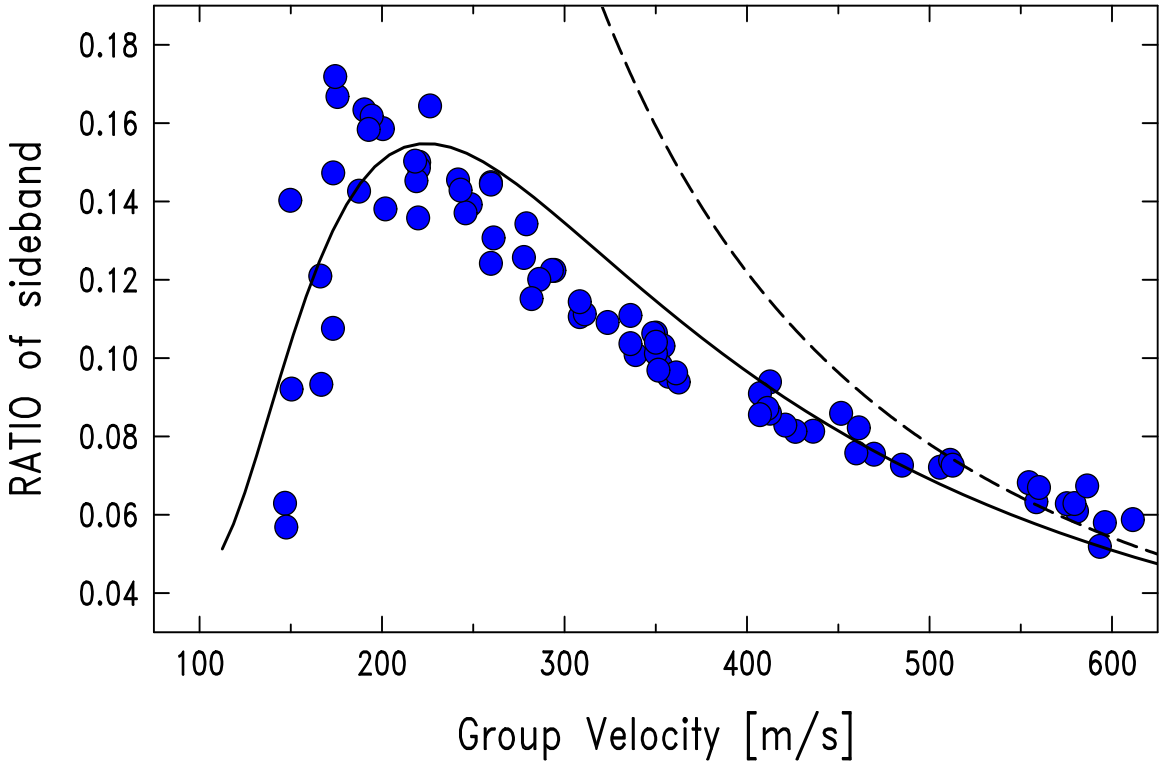

Fig. 18. Dependence of the sideband ratio on the group velocity of the probe field. Solid points are experimental data and the solid line is the result of our numerical simulations discussed in the text. The dashed line is the prediction of Eq. (4.27). Both coupling and probe lasers are on resonance, and the frequency of the sound wave is 1.5 kHz.

sideband intensities as functions of two photon detuning. From the figures, we can see clearly the EIT window. If the two photon tuning is outside of the EIT window, sidebands are being absorbed.

D. Enhanced coupling due to dragging effect

To fully explain observed results, one should take into account many parameters of the system: inhomogeneous Doppler broadening of the atomic transitions in vapor, homogeneous broadening due to collisions with the buffer gas, the amplitude of the sound wave excited in the cell leading to modulation of the density of Rb atoms in space and time, the motion of the cell as a whole, which together with the sound

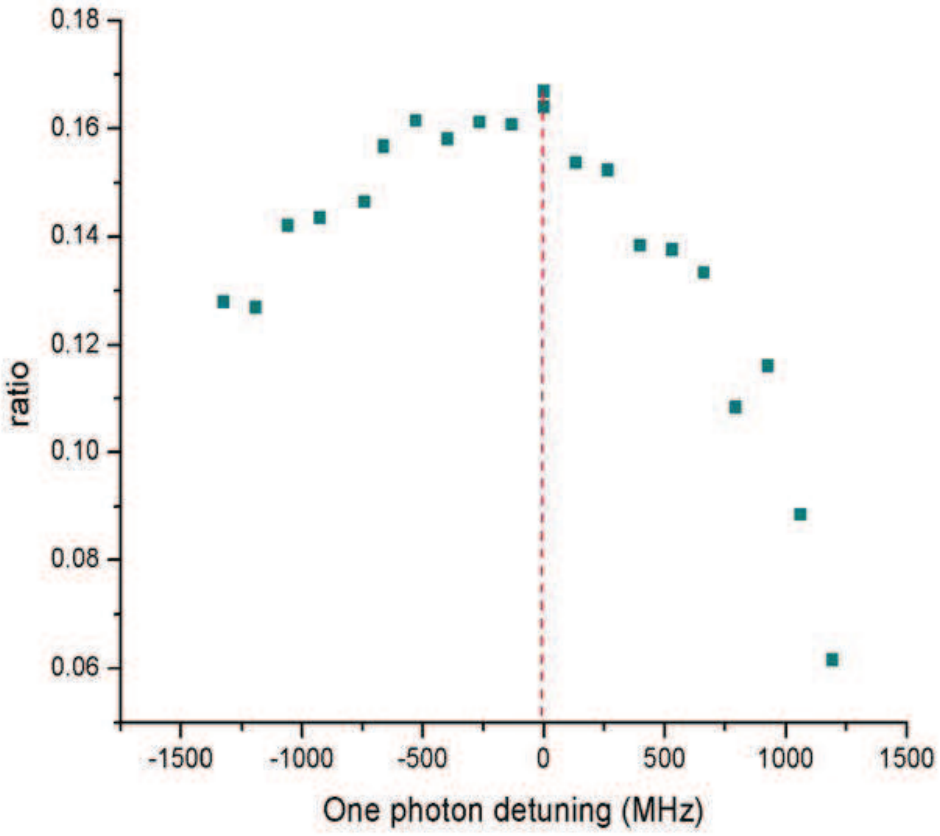

Fig. 19. Dependence of the sideband ratio on one photon detuning of probe field with Rb cell temperature at 65.0°C, with the density of Rb atom $1.1 \times 10^{11}[1/\mathrm{cm}^3]$.

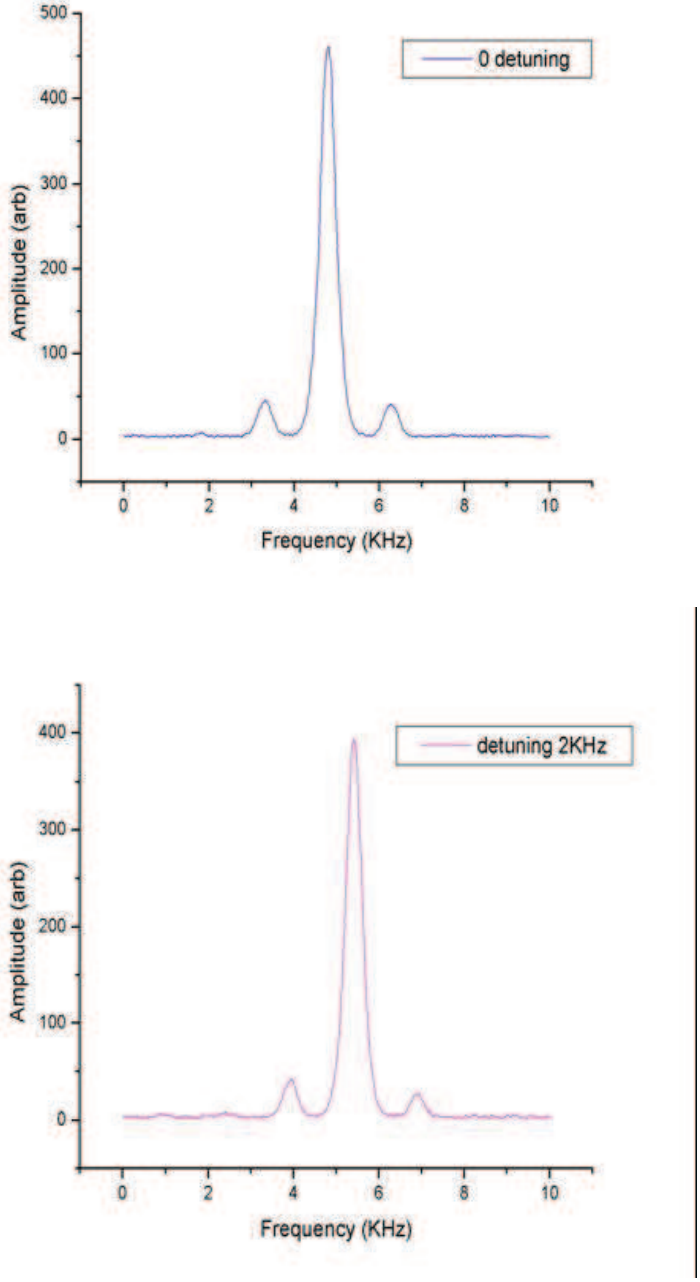

Fig. 20. Dependence of the generated sideband intensities on two photon detuning of probe field with Rb cell temperature at 65.0°C, with the density of Rb atom $1.1 \times 10^{11}[1/\mathrm{cm}^3]$.

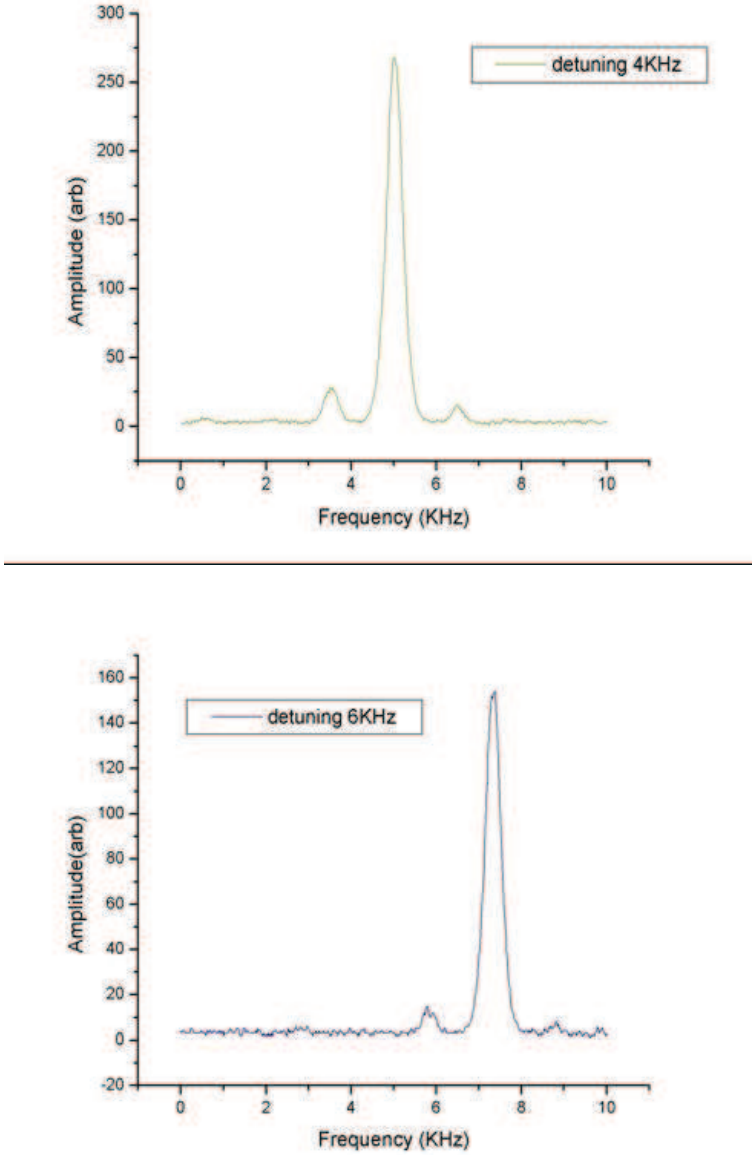

Fig. 20. Continued. Dependence of the generated sideband intensities on two photon detuning of probe field with Rb cell temperature at 65.0°C, with the density of Rb atom $1.1 \times 10^{11}[1/\mathrm{cm}^3]$.

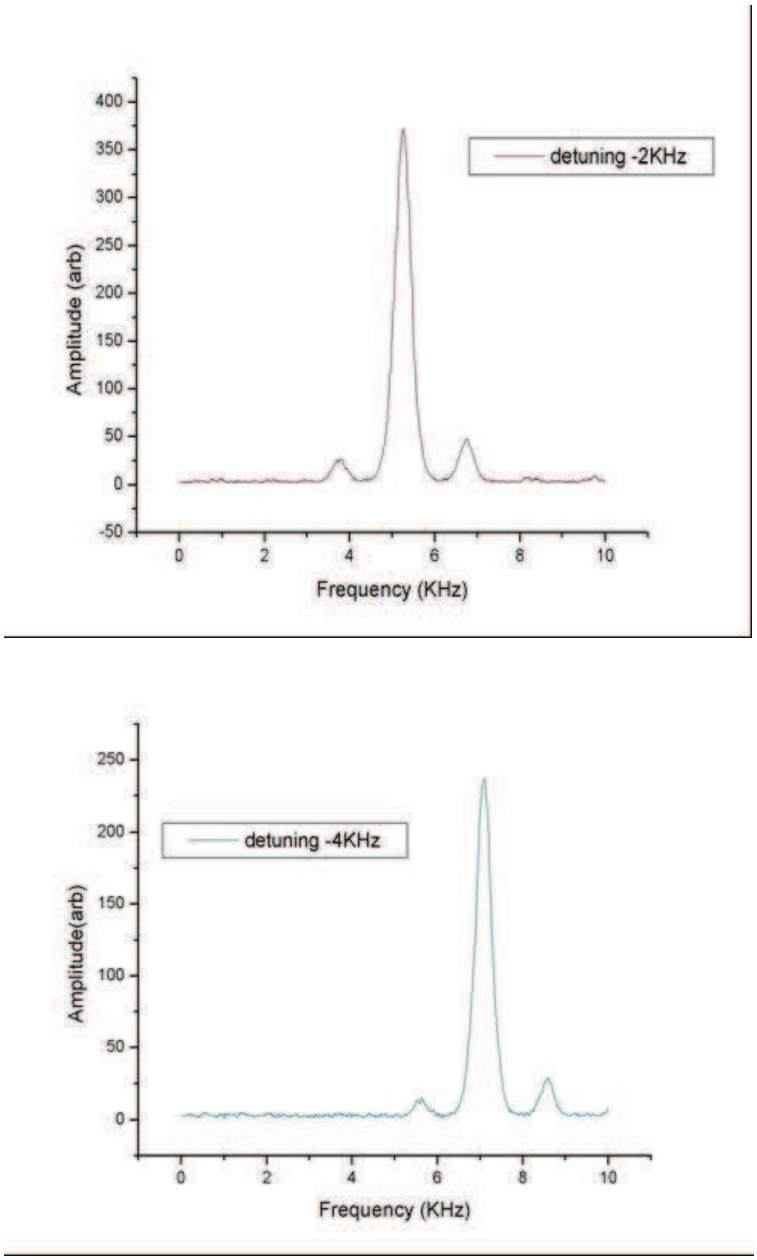

Fig. 20. Continued. Dependence of the generated sideband intensities on two photon detuning of probe field with Rb cell temperature at 65.0°C, with the density of Rb atom $1.1 \times 10^{11}[1/\mathrm{cm}^3]$.

wave leads to additional frequency detuning due to the Doppler effect by the regular motion of Rb gas.

First we consider the effect of phase matching on the interaction between the light and sound wave. The phonon-photon interaction Hamiltonian is given by

$$H_{int} = g\frac{\sin \Delta kL}{\Delta kL}\hat{a}_1\hat{a}_2^{+}\hat{b} + \text{adjoint} \tag{4.13}$$

where g is the coupling constant, L is the length of the cell, $\hat{a}_1$, $\hat{a}_2$, and $\hat{b}$ are the annihilation operators of the EM fields and acoustic phonon. The phase-matching condition for two co-propagating optical EM waves (with wave numbers $k_{1,2}$ and frequencies $\omega_{1,2}$) interacting with an acoustic wave (with wave number k_b and frequency ω_b) is $\Delta k = k_1 - k_2 - k_b = 0$. Conservation of energy requires:

$$\omega_1 - \omega_2 = \omega_b \tag{4.14}$$

Since $\omega_b \ll \omega_{1,2}$, we may write

$$\begin{aligned} k_1 - k_2 &= \frac{\omega_1 n(\omega_1)}{c} - \frac{\omega_2 n(\omega_2)}{c} \\ &= \frac{\omega_1 - \omega_2}{c}\frac{\partial[\omega n(\omega)]}{\partial\omega} \\ &= \frac{\omega_1 - \omega_2}{V_g} \end{aligned}$$

and $k_b = \omega_b/V_s$ where $V_g = c/[\partial(\omega n(\omega))/\partial\omega]$ and V_s are the EM group and the sound velocities respectively. If the condition $\omega_b = \omega_1 - \omega_2$ is satisfied and the condition $V_g = V_s$ is met, phase matching is achieved. However, from Fig. 18 we see that nothing special occurs at the point where the group velocity equals the sound speed (480 ms^{-1} in our experiment). We conclude that because the length of the cell (2 cm) is much less than a sound wavelength (20 cm) that phase matching is not critical to the interaction in our experiment.

Next we consider dispersion of the EM-wave brought about by the moving cell. Motion of the cell produces a drastic modification of the dispersion, changing both

the group and phase velocities of the light propagating through the cell [60]

$$V_g' = V_g + v \ , \qquad V_{ph}' = V_{ph}\frac{V_g}{V_g + v} \tag{4.15}$$

where V_g and V_g' are the group velocities of the light with respect to the cell at rest and with respect to the cell moving with velocity v, and similarly V_{ph} and V_{ph}' are the phase velocities of the light.

A useful physical picture can be gained in a frame fixed to the cell where the probe and coupling fields appear to be phase modulated due to motion of the cell. The perturbation of the phase is given by $\phi(t) = kz(t)$, where k is the wavenumber of the probe and/or coupling field ($k \simeq k_p \simeq k_d$) and $z(t)$ is the position of the cell as a function of time. Similarly, the change in the frequency is given by $\dot{\phi}(t) = kv(t)$, where $v(t) = a\omega_s \cos(\omega_s t)$ is the velocity of the cell. Then the probe and coupling fields have phase modulation and can be represented as

$$E_{p,d} = E_{p,d}^{\mathrm{lab},0} \exp[ikz(t)] \tag{4.16}$$

where the superscript $(\mathrm{lab}, 0)$ refers to the field in the laboratory frame (rather than the frame of the cell) at $z = 0$. Taking $z(t) = a\sin(\omega_s t)$ where a is the amplitude of oscillation of the cell, we have

$$E_{p,d} = E_{p,d}^{\mathrm{lab},0} \sum_q J_q(ka) e^{iq\omega_s t} \equiv \sum_q E_{p,d}^q \, e^{iq\omega_s t} \tag{4.17}$$

where the amplitudes of the sidebands at the entrance of the cell are given by $E_{p,d}^q = E_{p,d}^{\mathrm{lab},0} J_q(ka)$. Then the atomic system is driven by multi-frequency probe and coupling fields $E_{p,d}^q$. The interaction Hamiltonian can be written as

$$H = \hbar \left[|b\rangle\langle a| \Omega_p^* + |c\rangle\langle a| \Omega_d^* + adj. \right]$$

where $|a\rangle\langle a|$, $|c\rangle\langle c|$, $|b\rangle\langle a|$, and $|c\rangle\langle a|$ are the atomic projection operators, 2δ is the two-photon detuning, $\Omega_p = \wp_{ab} E_p/\hbar$ and $\Omega_d = \wp_{ac} E_d/\hbar$ are the probe and coupling

Rabi frequencies, and $\wp_{ab}$ and $\wp_{ac}$ are the dipole momenta of the transitions.

The coupling field is resonant with the $|a\rangle \rightarrow |c\rangle$ transition as shown in Fig. 13. Density matrix equations are given by

$$\frac{\partial \sigma}{\partial t} = \frac{i}{\hbar}[\sigma, H] - \frac{1}{2}(\Gamma\sigma + \sigma\Gamma) \tag{4.18}$$

where Γ is the matrix of relaxation rates for all components of the density matrix σ. Inside the cell, temporal and spatial evolution of the fields is determined by the propagation equations:

$$\frac{\partial \Omega_p}{\partial z} = -i\eta\sigma_{ab}, \qquad \frac{\partial \Omega}{\partial z} = i\eta\sigma_{ca} \tag{4.19}$$

After the cell, the transformation of the fields back to the lab frame is as follows

$$\Omega_{p,d}^{lab,L} = \Omega_{p,d}^{L} \exp[-ikz(t)] \tag{4.20}$$

where $\Omega_{p,d}^{L}$ denotes the Rabi-frequencies of the probe and coupling fields at the output of the cell.

After writing the atomic coherence in the form $\sigma_{ab} = \sum_q \sigma ab^q \exp[iq\omega_s t]$, $\sigma_{ca} = \sum_q \sigma_{ca}^q \exp[iq\omega_s t]$, $\sigma_{cb} = \sum_q \sigma_{cb}^q \exp[iq\omega_s t]$, and assuming that the coupling field is much stronger than the probe, the density matrix equation can solved to find

$$\sigma_{ca}^q = i\frac{n_{ca}}{\Gamma_{ca}}\Omega^q, \quad \sigma_{ab}^q = i\frac{n_{ab} + \frac{|\Omega_0|^2}{\Gamma_{ca}\Gamma_{cb}^q} n_{ca}}{\Gamma_{ab^q + \frac{|\Omega_0|^2}{\Gamma_{cb}^q}}}\Omega_p^q \tag{4.21}$$

where $\Gamma_{ca} = \gamma_{ca} - i(\omega_{ac} - \omega_d)$, $\Gamma_{cb}^q = \gamma_{cb} + i(\omega_{cb} - \omega_p + \omega_d - q\omega_s)$, and $\Gamma_{ab}^q = \gamma_{ab} + i(\omega_{ab} - \omega_p - q\omega_s)$. Assuming that the coupling field is strong enough to neglect its absorption, the probe field susceptibility is given by:

$$\chi_{ab}^q = i\eta\frac{n_{ab} + \frac{|\Omega_0|^2}{\Gamma_{ca}\Gamma_{cb}^q} n_{ca}}{\Gamma_{ab}^q + \frac{|\Omega_0|^2}{\Omega_{cb}^q}} \tag{4.22}$$

We can write the solution of the propagation equation for the probe field at the

output of the cell as:

$$\Omega_p^{q,L} = \Omega p^{0,q} \exp[\chi_{ab}^q(q\omega_s)L] \tag{4.23}$$

where $\chi_{ab}^q(q\omega_s) = i\eta\sigma_{ab}^q/\Omega_p^{0,q}$. Let us note that for the coupling field there is no modulation in the lab frame. Meanwhile, the side-bands of the probe field propagate with slow group velocity, and due to steep dispersion they acquire different phases which leads to phase modulation. Transforming back to the lab frame, we obtain:

$$\Omega_p^L = \sum_q \Omega_p^{q,L} \exp[iq\omega_s t] \exp[-ikz(t)], \tag{4.24}$$

and the ratio of the amplitudes of the sidebands of the q-th order to the central can be written as follows

$$\frac{\Omega_p^{L,q}}{\Omega_p^0} = \frac{J_q(ka)}{J_0(ka)} \left(\exp\left[\chi_{ab}^q(q\omega_s)L - \chi_{ab}^0 L\right] - 1\right) . \tag{4.25}$$

Similarly, for the intensity of the sidebands, we find

$$(\frac{\Omega_p^{L\pm}}{\Omega_p^0})^2 = (\frac{J_1(ka)}{J_0(ka)})^2 \sin^2(\chi_{ab}^{\pm}(\pm\omega_s)L - \chi_{ab}^0 L^2) \tag{4.26}$$

Simplifying the above expression we obtain for the intensity of the first sidebands, we find

$$\left(\frac{\Omega_p^{\pm}}{\Omega_p^0}\right)^2 = \frac{1}{16}\left(\frac{ka\omega_s L}{V_g}\right)^2 . \tag{4.27}$$

We note that the modulation we are describing has its origin in the effect of light dragging [60]. The prediction of Equ.(4.27) is plotted in Fig. 18. We see that the agreement with experiment is not convincing as we lower the group velocity. We understand this disagreement as the result of absorption, which is not included in this simple calculation.

In order to obtain better agreement, we perform numerical calculations of the dependence of the magnitude of the first side bands versus coupling laser power, using parameters from the experiment. This simulation includes the propagation of

both probe and coupling fields through the cell, as described in Ref. [34] [61]. The result is shown in Fig. 18. As one can see, the simulations give good agreement with experimental results.

E. Summary

High efficiency of sidebands generated by acoustic modulation of a material transmitting slow light is shown. The motion affects the phase velocity and the modification of phase velocity is due to the motion of the Rb cell. This experimental results bolster the theoretical predictions in [58]. We have shown that the physics behind this sideband appearance is due to the dragging effect which is similar to the prediction [62] and recently experimental observation of modification of the group velocity due to atomic motion [63],. Our results may lead to observation of forward stimulated Brillouin scattering and effective squeezing.

Furthermore, since our observed modulation is large (order of 10%) and considering the relatively small amount of atoms is involved, this may have applications to efficient modulators. Since the velocity of the cell in our experiments is small (order of 1 cm/s), this technique can be used to detect small velocities. Our results can be easily extended to solids which give more application where ultra slow light has been efficiently demonstrated.

CHAPTER V

SPATIAL CONSEQUENCES AND OPTICAL STEERING VIA SLOW LIGHT

A. Introduction and principle of experiment

A particularly interesting consequence of nonlinear processes such as EIT is the spatial effects due to the interaction of light and matter. As we all know, optical beam deflection has many applications in modern optics. It is important for free space communication and optical imaging applications. Recently, optical beam deflection by another beam of light via interaction with matter has drawn attention because of its fast response compared to other mechanisms.

Many physical mechanisms have been applied to achieve light beam a basic and convenient method. Besides this traditional method, acoustic-optical interaction [64] [65] and electro-optical effects [66] can also deflect the light beam. Nowadays, EIT mechanism used in optical beam deflection has been studied by several groups. Moseley et al. first reported the electromagnetic induced focusing and defocusing effect in rubidium vapor [67], in which deflection comes both from refraction and absorption modification effects inside a gaussian spatial distribution of the pump field. This also can lead to electromagnetically induced focusing and defocusing by scanning the probe laser field. Using EIT to control the path of one propagating beam by another is nondissipative in terms of the drive field. Also, EIT allows focusing and defocusing with little absorption of the probe field is big plus. Sun et al [68] proposed a scheme providing all optical controlled steering of light using an inhomogeneous drive field and EIT. A semiclassical approach for light deflection by a coherent Λ-type three level atomic medium in either inhomogeneous magnetic field or inhomogeneous control laser field is presented by Zhou et al in 2007 [69]. A more recent experiment by Sautenkov et al., reports an ultra-dispersive optical prism in which beam deflection in coherent media with angular dispersion six orders of magnitude

higher than a classical glass prism [70].

Here we present a study of the large change in refractive index at the interface of a window and rubidium gas which results in optical beam deflection. Snell's law tells us that when light passes from one medium into another with a different index of refraction, part of the incident light is reflected at the boundary, and the remainder is bent, or refracts into the new medium. The angle of refraction depends on the speed of light in the media and also depends on the incident angle:

$$n_1 \sin\theta_1 = n_2 \sin\theta_2 \tag{5.1}$$

where θ_1 is the incident angle and θ_2 is the refractive angle, n_1 and n_2 are the respective indices of refraction of material. As we know,the index of refraction of a material depends on the frequency. Taking the incident refractive index to be 1 gives:

$$\sin\theta(\omega) = \frac{\sin\theta_0}{n(\omega)} \tag{5.2}$$

Therefore,

$$\delta\omega \frac{\delta\theta}{\delta\omega} \cos\theta(\omega) = -\frac{1}{n^2(\omega)} \sin\theta_0 \frac{\partial n}{\partial\omega}\delta\omega \tag{5.3}$$

$$\begin{aligned} \frac{\delta\theta}{\delta\omega} &= -\frac{1}{n^2(\omega)} \frac{\sin\theta_0}{cos\theta(\omega)} \frac{\partial n}{\partial\omega} \\ &= \delta\theta \cong -\frac{\delta\omega}{\omega}\frac{n_g}{n^2} tan\theta_0 \cong -\frac{\delta\omega}{\omega} n_g \tan\theta_0 \end{aligned}$$

with

$$n_g \cong n + \omega\frac{\partial n}{\partial\omega} \cong w\frac{\partial n}{\partial\omega} \tag{5.4}$$

From the above equation, we can see the refraction angle is proportional to n_g as related to the group velocity v_g. With ultra-slow light, large and measurable beam deflection is predicted for the EIT regime.

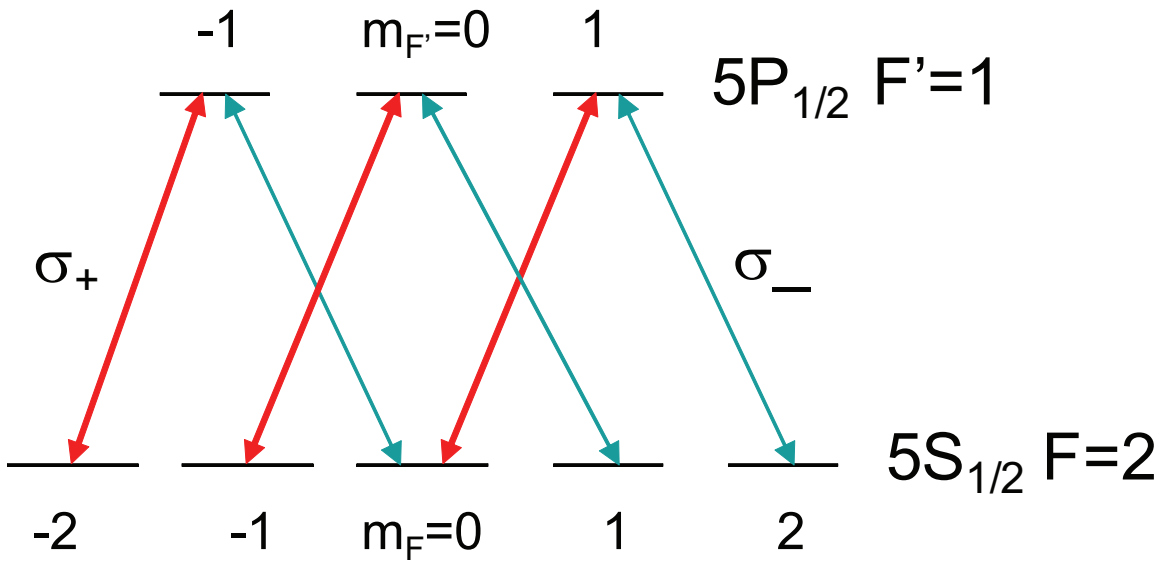

Fig. 21. Zeeman sublevel transitions of $^{87}Rb5^2S_{1/2}(F=2) \Rightarrow 5^2P_{1/2}(F'=1)$ under consideration with two opposite circular polarization laser fields

B. Slow light measurement

To observe beam deflection in Rb gas medium, low group velocity should be achieved first. In this experiment, a Λ configuration is used on the Rb D1 line $5^2S_{1/2}(F=2) \Rightarrow 5^2P_{1/2}(F'=1)$. Using the same frequency but with opposite circular polarization for pump and probe, we couple different Zeeman sublevels of the ground state. EIT resonance is observed in the Λ configuration system by applying and scanning a longitudinal magnetic field. The Λ type three level system is made up of two groups of states from the Zeeman sublevels of the $5^2S_{1/2}(F=2)$. We use commercial diode laser system which is tuned to the transition Rb D1 line $5^2S_{1/2}(F=2) \Rightarrow 5^2P_{1/2}(F'=1)$. These levels are coupled by two optical fields with one strong pump field and one weak probe field. To measure the group velocity of the probe field, an acoustic-optical modulator is inserted into the probe beam to modulate its intensity. The Zeeman sublevels of these transition are shown Fig. 21.

A schematic of the experimental setup is shown in Fig. 22. The Rb vapor cell contains isotopically enhanced ^{87}Rb and 30 torr Neon buffer gas. The length of the

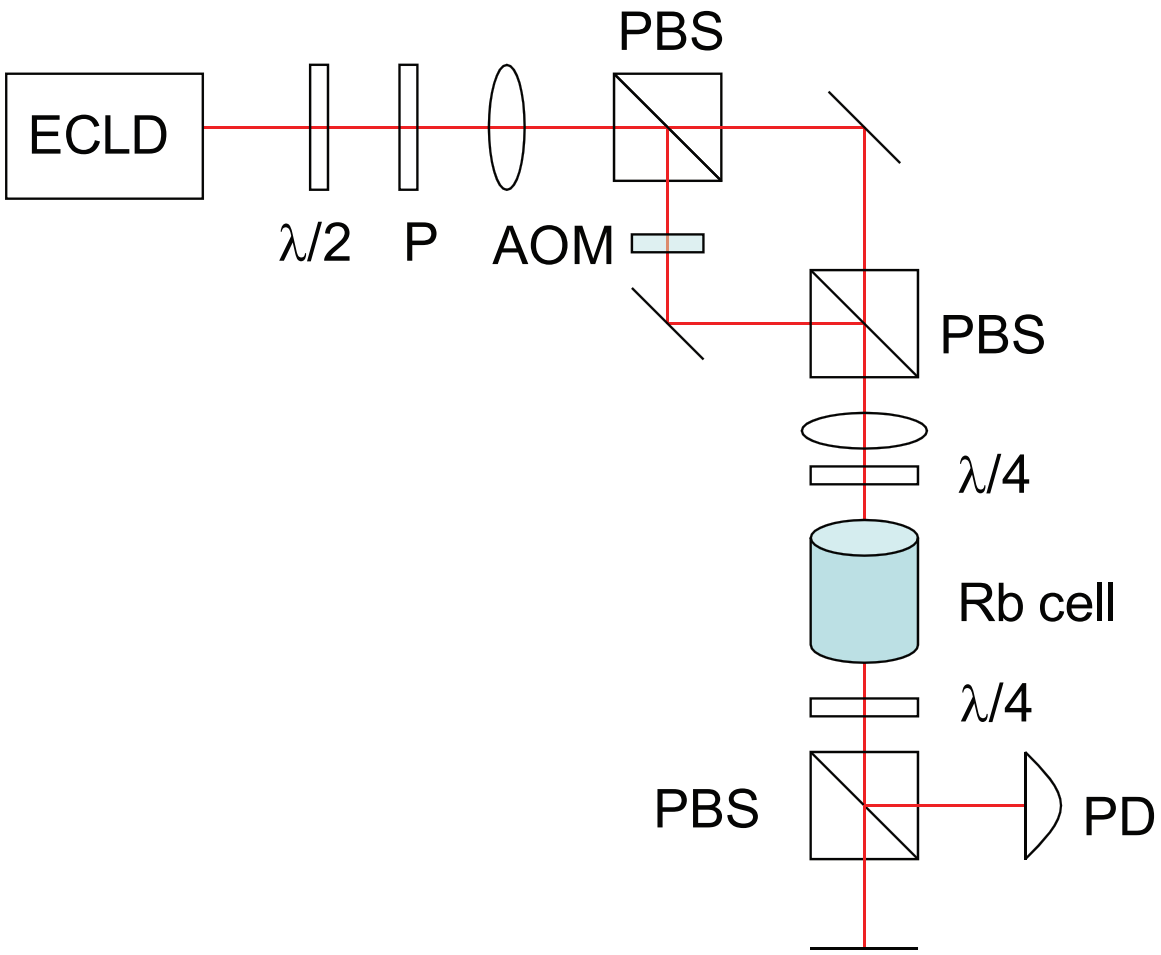

Fig. 22. A schematic of experimental setup for group velocity: ECDL is external cavity diode laser, PBS is polarization beamsplitter, $\lambda/2$ is half wave plate, $\lambda/4$ is quarter wave plate, PD is photodiode detector, P is polarizer, AMO is acoustic modulator

cell is 2.5 cm. A two layer magnetic shield is used to reduce the stray magnetic field near the cell. The Rb vapor density is controlled by the temperature of cell. An acoustic modulate the amplitude of the probe field. By looking at the time delay between the modulated transmitted and incident probe field, we can measure the group velocity. The method is similar to that described in Chapter IV.B. The lowest group velocity we have measured is 42 ms^{-1} with an EIT width about 460 Hz at Rb density $7.3 \times 10^{11}[1/cm^3]$ with probe field power 2.02 μW and drive field power 86.6 μW .

C. Experimental setup and result

A schematic of the experimental setup to measure beam steering is shown in Fig. 23. Linearly polarized output from driving laser can be considered as two equal amplitude circular polarization components to couple to different Zeeman sublevels. Similarly, an elliptically polarized field can be considered to be composed of two different amplitude circular polarization components. Therefore, using one elliptically polarized field we can create an EIT coherent superposition in Zeeman sublevels. Additionally, using one beam instead of two allows us to eliminate beam deflection such as that was done by Sautenkov et al. [70], in which they control the direction of light propagation by another light beam.

The powers of pump and probe fields are controlled by adjusting the half-wave plate. The polarizations of both fields can be varied by rotating the polarizer and quarter-wave plate. After the Rb cell the probe beam is separated with a quarter wave plate and polarized beam splitter. By scanning the magnetic field and recording both the transmission and direction of the circularly polarized probe field, the EIT signal and steering angle can be measured simultaneously by two different photo detectors.

A single-mode optical fiber is used to get a good gaussian beam profile. After the fiber, our laser beam is about 4 mm beam diameter with linear polarization. A half

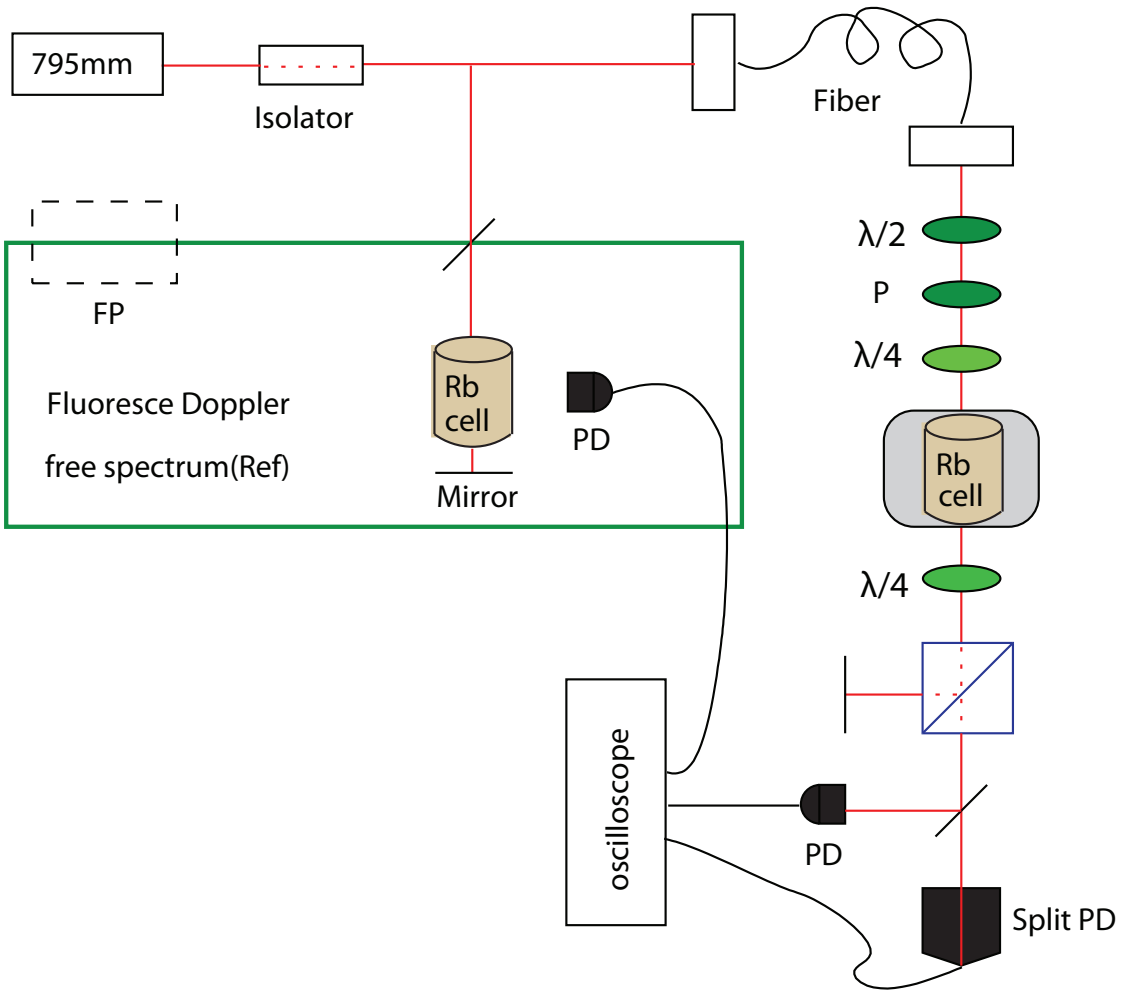

Fig. 23. A schematic of experimental setup: P is polarizer, $\lambda/2$ is half wave plate, $\lambda/4$ is quarter wave plate, PD is photodiode detector.

wave plate before the polarizer is used as to control the pump and probe power. Before we put the cell into the setup, the polarizer is lined with the polarization beam splitter. Then the second quarter wave plate is also lined with the polarization beam splitter. Using the half wave plate and a quarter wave plate, we can keep the amplitude of probe field the same but with varying pump field. A polarization beam splitter is put into setup to separate the pump and probe beam after Rb cell. A photodiode detector is used to monitor the amplitude, and a position sensitive detector (split photodiode) measures the position of the probe beam. The split photodetector is placed at a distance of 45 cm from the center of Rb cell.

First, the transmission of the probe (EIT) signal is measured by changing with the pump power at shown in the experimental setup of Fig. 23. We find the range in which the group velocity less than 100 m/s, which typically means the EIT width (FWHM) less than 1 kHz. Fig. 24 give the dependence of EIT width on the input power of the optical fields at three different rubidium densities. For high density, the signal is noisy due to the weak transmitted probe field after strong absorption of the medium. The EIT width (FWHM) less than 1 kHz can be found at relatively low density with a probe field.

Both the transmission and direction signals of the probe field are measured simultaneously as shown in in Fig. 25 by scanning the magnetic field of the system with total input optical field 151.7μW.

D. Conclusion

In conslusion, we have measured the properties of EIT resonances as a function of input power of pump and probe fields at Rb vapor medium. Ultra-slow group velocity less than 100ms^{-1} has been measured using different polarization of light and Zeeman sublevels. We have experimentally demonstrated the large light beam deflection at the interface between cell glass and Rb medium due to the ulra-dispersive EIT region.

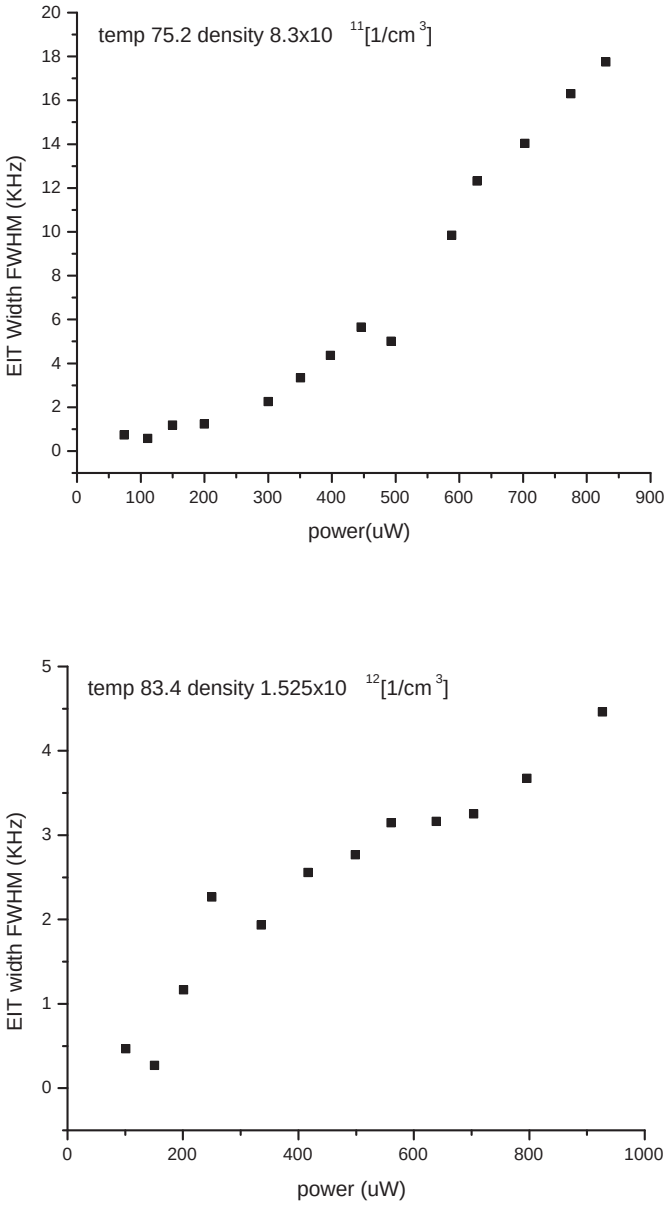

Fig. 24. Dependence of EIT width of input power of pump and probe optical fields with probe and pump field ratio at $1 : 2.55$. These dependences are measured at different Rb atomic densities.

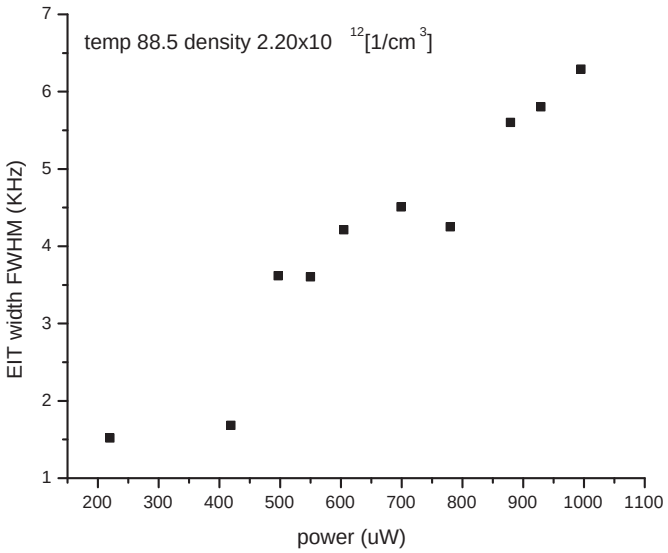

Fig. 24. Continued. Dependence of EIT width of input power of pump and probe optical fields with probe and pump field ratio at 1 : 2.55. These dependences are measured at different Rb atomic densities.

The obtained results shows the dependence of probe field traveling angles on the detuning that is introduced by the magnetic field. This result can have applications in optical imaging and all optical light steering.

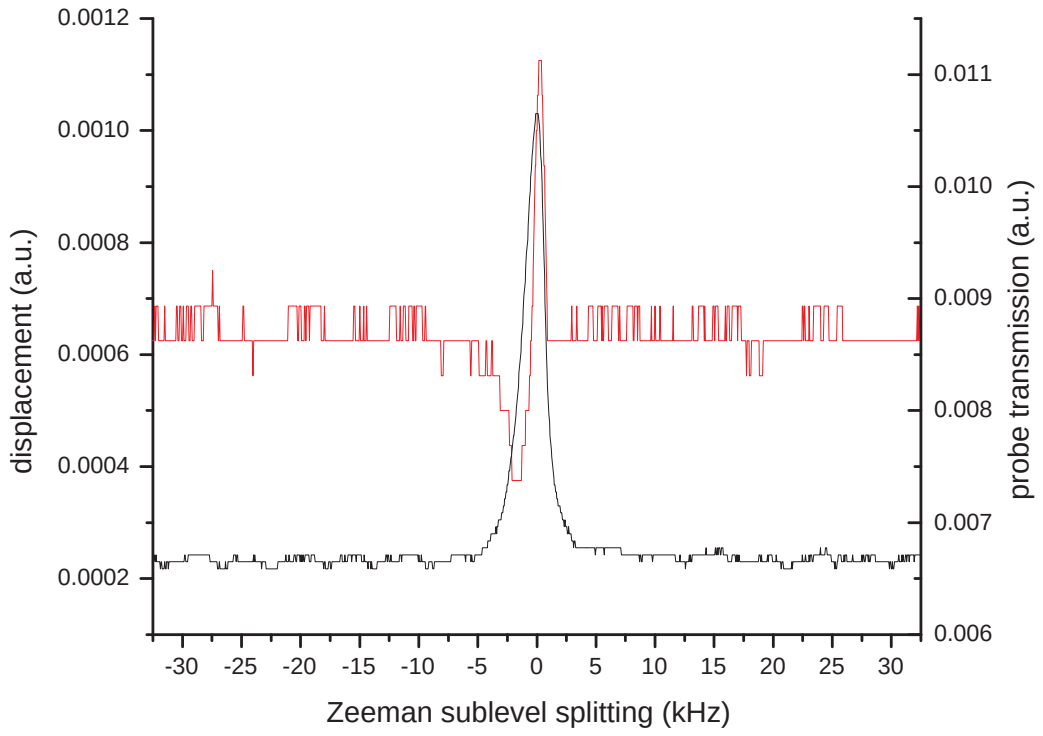

Fig. 25. Dependence of angle of the probe beam refraction and transmission of the probe field on the magnetic field at Rb density $6.06 \times 10^{11}[1/\mathrm{cm}^3]$.

CHAPTER VI

CONCLUSION

The main results of this work are the following:

A mode-locked rubidium laser was first time studied and experimental demonstrated at rubidium transition D1 line. The three level end-pumped laser oscillator which is based on rubidium fine structure energy level population inversion has large gain for laser output. An EOM was introduced to lock different cavity modes with modulation frequency equal to cavity mode separation. Quantum coherent effect: EIT has been demonstrated in different Zeeman levels using mode-locked rubidium laser fields. Nonlinear Faraday effect has been observed in ground-state Zeeman sublevels.

Enhanced coupling between optical and sound waves in forward direction was experimental demonstrated in rubidium vapor. The motion of the Rb cell affects the phase velocity, which modified the phase velocity results in sideband. Our results may lead to observation of forward stimulated Brillouin scattering and effective squeezing.

Ultra-slow group velocity less than 100 ms^{-1} has been measured in ground-state Zeeman sublevels system with two opposite polarizations of light. Several orders of magnitude enhancement of the light beam deflection has been experimentally demonstrated at the interface between cell glass and Rb medium.

REFERENCES

[1] O. A. Kocharovskaya, Y. I. Khania, Zh. Eksp. Teor. Fiz. **90** 1610 (1986); K. J. Boller, A. Imamoglu, S. E. Harris, Phys. Rev. Lett. **66**, 002593 (1991); S. E. Harris, Phys. Today **7**, 36, (1997)

[2] J. Kitching, L. Hollberg, S. Knappe, R. Wynands, Electron. Lett. **37**, 1449 (2001); J. Kitching, H. G. Robinson, L. Hollberg, S. Knappe, R. Wynands, J. Opt. Soc. Am. B. **18**, 1676 (2001); S. Knappe, Appl. Phys. Lett. **85**, 1460 (2004).

[3] M. D. Lukin, M. Fleischhauer, A. S. Zibro, H. G. Robinson, V. L. Velichansky, L. Hollberg, and M. O. Scully, Phys. Rev. Lett. **79**, 2959 (1997); s. Brandt, A. Nagel, R. Wynands, and D. Meschede, Phys. Rev. A. **56**, R1063 (1997); M. O. Scully, Phys. Rev. Lett. **67**, 1855 (1991); M. O. Scully, M. Fleischhauer, ibid. **69**, 1360 (1992); L. Arissian, J. Jones, J. C. Diels, J. Mod. Opt. **49**, 2517 (2002)

[4] H. Schmidt, A. Imamoglu, Opt. Lett. **21**, 1936 (1996); H. Wang, D. Goorskey, M. Xiao, Phys. Rev. Lett. **87**, 073601 (2001); A. Joshi, M. Xiao, Phys. Rev. A. **72**, 062319 (2005)

[5] G. Alzetta, A. Gozzini, L. Moi, and G. Orriols, Nouvo Cimento Soc. Ital. Fis. B-Gen. Phys. Relative. Astron. Math. Phys. Methods. **36**, 5 (1976)

[6] A. S. Zibrov, M. D. Lukin, L. Hollberg, D. E. Nikonov, M. O. Scully, H. G. Robinson, V. L. Velichansky, Phys. Rev. Lett. **76**, 3935 (1996).

[7] S. Harris, A. Sokolov, Phys. Rev. Lett. **81**, 2894 (1998).

[8] J. Kitching, L. Hollberg, Phys. Rev. A. **59**, 4685 (1999).

[9] K. Winkler, G. Thalhammer, M. Theis. R. Grimm, J. Hecker Denschlag. Phys. Rev. Lett. **95**, 063202 (2005).

[10] B. S. Ham, P. R. Hemmer, M. S. Shahriar. Opt. Commun. **144**, 227 (1997)

[11] R. Kolesov, Phys. Rev. A. **72**, 051801 (2005)

[12] A. Imamoglu, Opt. Commun. **179**, 179 (2000)

[13] M. O. Scully and M. Fleischhauer, Phys. Rev. Lett. **69**, 1360 (1992)

[14] R. Wynands and A. Nagel, Appl. Phys. B. **68**, 1 (1998)

[15] S. Knapper, R. Wynands, J. Kitching, H. G. Robinson and L. Hollberg, J. Opt. Soc. Am. B-Opt. Phys. **18**, 1545 (2001)

[16] M. Fleischhauer, A. Imamoglu, J. P. Marangos, Rev. Mod. Phys. **77**, 633, (2005)

[17] S. E. Harris, J. E. Field and A. Kasapi, Phys. Rev. A. **46**, R29 (1992)

[18] M. M. Kash, V. A. Sautenkov, A. S. Zibrov, L. Hollberg, G. R. Welch, M. D. Lukin, Y. Rostovtsev, E. S. Fry and M. O. Scully, Phys. Rev. Lett. **82**, 5229 (1999)

[19] A. Godone, F. Levi and S. Micalizio, Phys. Rev. A. **66**, 043804 (2002)

[20] L. V. Hau, S. E . Harris, Z. Dutton and C. H. Behroozi, Nature **397**, 594 (1999)

[21] A. V. Turukhin, V. S. Sudarshanam, M. S. Shahriar, J. A. Musser, B. S. Ham, and P. R. Hemmer, Phys. Rev. Lett. **88**, 023602 (2002)

[22] D. Budker, D. F. Kimball, S. M. Rochester and V. V. Yashchuk, Phys. Rev. Lett. **83**, 1767 (1999)

[23] M. S. Bigelow, N. N. Lepeshkin, and R. W. Boyd, Phys. Rev. Lett. **90**, 113903 (2003)

[24] E. Podivilov, B. Sturman, A. Shumelyuk and S. Odoulov, Phys. Rev. Lett. **91**, 083902 (2003)

[25] D. F. Phillips, A. Fleischhauer, A. Mair, R. L. Walsworth and M. D. Lukin, Phys. Rev. Lett. **86**, 783 (2001)

[26] C. Liu, Z. Dutton, C. H. Behroozi, L. V. Hau, Nature **409**, 490 (2001)

[27] A. S. Zibrov, A. B. Matsko, O. Kocharovskaya, Y. V. Rostovtsev, G. R. Welch, M. O. Scully, Phys. Rev. Lett. **88**, 103601 (2002)

[28] J. T. Manassah and I. Gladkova, Laser Phys. **11**, 801 (2001)

[29] J. D. Jackson, *Classical Electrodynamics*(Wiley, New York, 1962)

[30] R. Shanker *Principle of Quantum Mechanics* (Springer, New York and London, 1994)

[31] M. O. Scully and M. S. Zubairy, *Quantum Optics* (Cambridge University Press, Cambridge, England, 1997)

[32] J. P. Marangos J. Mod. Opt. **45**, 471 (1997)

[33] M. Fleischhauer, A. Imamoglu, J. P. Marangos, Rev. Mod. Phys. **77**, 633 (2005)

[34] E. E. Mikhailov, Y. V. Rostovtsev, G. R. Welch, J. Mod. Opt. **50**, 2645 (2003)

[35] A. Javan, O. Kocharovskaya, H. Lee, M. O. Scully, Phys. Rev. A. **66**, 013805 (2003)

[36] H. Lee, Y. Rostovtsev, C. J. Bednar, A. Javan, Appl. Phys. B. **76**, 33 (2003)

[37] S. Brandt, A. Nagel, R. Wynands, D. Meschede, Phys. Rev. A. **56**, R1063 (1997)

[38] M. Erhard, H. Helm, Phys. Rev. A. **63**, 043813 (2001)

[39] D. Budker, V. Yashchuk, M. Zolotorev, Phys. Rev. Lett. **81**, 5788 (1998)

[40] E. B. Alexandrov, M. V. Balalbas, D. Budker, D. S. English, D. F. Kimball, C. H. Li, V. Yashchuk, Phys. Rev. Lett. **66**, 042903 (2002)

[41] T. H. Maiman, Nature (Lond.) **187**, 493 (1960)

[42] M. Sargent III, M. O. Scully, W. E. Lamb, Jr. *Laser Physics*(Addison-Wesley, Reading, MA. 1974)

[43] G. Cerullo, S. Longhi, M. Nisoli, S. Stagira, O. Svelto, *Problems in Laser Physics*(Springer, New York, 2001)

[44] W. Demtrder, *Laser Spectroscopy*(Springer-Verlag, New York, 1996)

[45] W. F. Krupke, R. J. Beach, V. K. Kanz, S. A. Payne. Opt. Lett. **28**, 2336 (2003)

[46] R. H. Page, R. J. Beach, V. K. Kanz, W. F. Krupke. Opt. Lett. **31**, 353 (2006)

[47] S. Q. Wu, T. F. Soules, R. H. Page, S. C. Mitchell, V. K. Kanz, R. J. Beach. Opt. Lett. **32**, 2423 (2007)

[48] V. A. Sautenkov, Y. V. Rostovtsev, C. Y. Ye, G. R. Welch, O. Kocharovskaya, M. O. Scully, Phys. Rev. A. **71**, 063804 (2005)

[49] L. Arissian, J. C. Diels., Opt. Comm. **264**, 169 (2006)

[50] A. Weis, V. A. Sautenkov, T. W. Hänsch. Phys. Rev. A. **45**, 7991 (1992)

[51] I. Novikova, G. R. Welch, J. Mod. Opt. **49**, 349 (2001)

[52] M. V. Romalis,E. Miron, G. D. Cates. Phys. Rew. A. **56**, 4569 (1997)

[53] E. Walentynowiz, R. A. Phabeup, L. Krause. Can. J. Phys. **52**, 589 (1974)

[54] Z. Konefal. Opt. Comm. **164**, 95 (1999)

[55] G. Alzetta, L. Moi.IL. NUOVO CIMENTO. **52**, 209 (1979)

[56] V.A. Sautenkov, Yu. Rostovtsev and M.O. Scully, Phys. Rev. A **72**, 065801 (2005)

[57] V.A. Sautenkov, H. Li, Yu. Rostovtsev and M.O. Scully, J. Mod. Opt. **54**, 2451 (2007)

[58] A. B. Matsko, Y. V. Rostovtsev, M. Fleischhauer, M. O. Scully Phys. Rev. Lett. **86**, 2006 (2001)

[59] A. B. Matsko, Y. V. Rostovtsev, H. Z. Cummins, M. O. Scully, Phys. Rev. Lett. **84**, 5752 (2000)

[60] L. D. Landau, E. M. Lifshitz, *Electrodynamics of continuous media*(Pergamon Press, Oxford, England 1960)

[61] E. E. Mikhailov, I. Novikova, Y. V. Rostovtsev, G. R. Welch, Phys. Rev. A. **70**, 033806 (2004)

[62] O. Kocharovskaya, Y. Rostovtsev, M. O. Scully Phys. Rev. Lett. **86**, 628 (1999)

[63] D. Strekalov, A. B. Matsko, N. Yu, L. Maleki, Phy. Rev. Lett. **93**, 023601 (2004)

[64] R. W. Dixon, J. Appl. Phys. **38**, 5149 (1967)

[65] D. A. Pinnow, IEEE J. Quantum Electron. **6**, 223 (1970)

[66] T. C. Lee, J. D. Zook, IEEE J. Quantum Electron. **4**, 442 (1968)

[67] R. R. Moseley, S. Shepherd. D. J. Fulton, B. D. Sinclair, M. H. Dunn, Phys. Rev. Lett. **74**, 670 (1995)

[68] Q. Q. Sun, Y. V. Rostovtsev, M. S. Zubairy. Phys. Rev. A. **74**, 033819 (2006)

[69] D. L. Zhou, L. Zhou, R. Q. Wang, S. Yi, C. P. Sun Phys. Rev. A. **76**, 055801 (2007)

[70] V. A. Sautenkov, H. Li, Y. V. Rostovtsev, M. O. Scully, e-print arXiv:quant-ph/0701229

[71] E. E. Mikhailov, Ph.D. dissertation, Texas A&M University, College Station (2003)

VITA

Name: Aihua Zhang

Address: Department of Physics, Texas A&M University
College Station, TX, 77843 – 4242

E-mail: azhang@physics.tamu.edu

Education:

May, 2009	Ph.D. Physics
	Texas A&M University, College Station, TX, USA
June, 2001	M.S. Applied physics
	Shanghai Jiaotong University, Shanghai, China
June, 1998	B.S. Electric light sources and illuminating engineering
	Fudan University, Shanghai, China

Experience:

2002 – 2009	Research Assistant
	Texas A&M University, Department of Physics
2001 – 2002	Product Development Engineer
	Philips Lighting Electronic (Shanghai), Competence Center
1998 – 2001	Research Assistant
	Shanghai Jiaotong University, Applied Physics Department
1997	Intern
	GE Lighting (Shanghai), Technology Center

The typist for this dissertation was Aihua Zhang.